SERI/STR-211-2845
(DE85016875)

RESEARCH ON HIGH-EFFICIENCY, STACKED, MULTI-JUNCTION, AMORPHOUS SILICON ALLOY THIN-FILM SOLAR CELLS

A Semiannual Subcontract Progress Report for the Period October 1, 1984–May 15, 1985

By
V. Dalal

November 1985

Work Performed Under Contract No. AC02-83CH10093

Spire Corporation
Bedford, Massachusetts

and

Solar Energy Research Institute
Golden, Colorado

Technical Information Center
Office of Scientific and Technical Information
United States Department of Energy

DISCLAIMER

Available from the National Technical Information Service, U. S. Department of Commerce, Springfield, Virginia 22161.

Price: Printed Copy A04
Microfiche A01

Codes are used for pricing all publications. The code is determined by the number of pages in the publication. Information pertaining to the pricing codes can be found in the current issues of the following publications, which are generally available in most libraries: *Energy Research Abstracts (ERA); Government Reports Announcements* and Index *(GRA* and I); *Scientific and Technical Abstract Reports (STAR);* and publication NTIS-PR-360 available from NTIS at the above address.

Printed in the United States of America
USDOE Office of Scientific and Technical Information
Oak Ridge, Tennessee

SERI/STR-211-2845
(DE85016875)
Distribution Category UC-63

Research on High-Efficiency, Stacked, Multijunction, Amorphous Silicon Alloy Thin-Film Solar Cells

A Semiannual Subcontract Progress Report 1 October 1984 - 15 May 1985

V. Dalal, Principal Investigator
Spire Corporation
Bedford, Massachusetts

November 1985

Prepared under Subcontract No. ZB-4-03055-1
SERI Technical Monitor: W. Luft

Solar Energy Research Institute
A Division of Midwest Research Institute

1617 Cole Boulevard
Golden, Colorado 80401

Prepared for the
U.S. Department of Energy
Contract No. DE-AC02-83CH10093

TABLE OF CONTENTS

LIST OF ILLUSTRATIONS (Concluded)

Figures

Tables

LIST OF ILLUSTRATIONS

ACKNOWLEDGEMENTS

The following personnel participated in the research reported in this report:

Spire Corporation:	Vikram Dalal, Program Manager and Principal Investigator
	Anton Greenwald
	Ashok Vaseashta
	James Booker
	Mark Leonard
	Mark Comeau
Polaroid:	Camille Fuleihan
	Charles Botts
	Floyd Berry
University of Delaware:	William Baron
	Steven Hegedus
	Kenneth Schubert

ABSTRACT

This technical progress report to the Solar Energy Research Institute covers work on high-efficiency, stacked, multijunction amorphous silicone alloy thin-film solar cells. Material growth was begun in a multisector reactor. The a-Si:H films grown in this reactor were very high quality, as shown in their high ratio of photo-to-dark conductivity and very low dark conductivity. High-band-gap a-Si:H films were achieved by using H etching of films during growth. H_2 dilution in the plasma led to a sharpening of the valence band tail in both a-Si:H and a-(Si,Ge):H films. No SiH_2 bonds were observed after Ge was added to the a-Si:H. Experiments were begun to develop a two-level, stable back contact to a-Si:H. Preliminary results indicate that a Cr/Pd contact may be stable and moderately reflecting, but the best reflection was obtained with Ag. Mo appears to be a suitable, stable contact to SnO_2. A critical parameter in achieving 8.5% efficient a-Si:H devices was plasma-cleaning between deposition of the p- and i-layers. 6.5% efficient a-(Si,Ge):H devices were also grown. Two types of tandem cells were fabricated.

SECTION I

SUMMARY

This is the third semi-annual technical progress report under the Solar Energy Research Institute supported program for "Research on High Efficiency Stacked Multi-Junction Amorphous Silicon Alloy Thin-Film Solar Cells". During the first half of Phase II of this program, the following progress was made.

1.1 MATERIAL GROWTH AND CHARACTERIZATION

Material growth was initiated in the multi-sector reactor. The quality of a-Si:H films grown in this reactor is very high, as indicated by a very high ratio of photo-to-dark conductivity ($>2x10^6$), and a very low dark conductivity ($\leq 10^{-11}$ Scm^{-1}). It was found that plasma cleaning of the sector (in which the i layer is grown) with SiH_4 prior to growth was a very effective cleaning mechanism that allowed growth of high quality films.

We have achieved growth of high-gap a-Si:H films by using H etching of films during growth. We find that diluting SiH_4 with H_2 in the plasma, combined with a negative bias on the substrate, leads to films with E_g=1.85 eV. Successful devices have been made with these films, with high V_{OC} (~0.88 V).

We have found that H_2 dilution in the plasma leads to a sharpening of the valence band tail (by about 4 meV) in both a-Si:H and a-(Si,Ge):H films. This result may be due to H etching of weak valence band states, leading to both an increase in E_g and a decrease in E_o, the characteristic energy for valence band tail states.

We have analyzed the H bonding in a-(Si,Ge):H alloys, using IR absorption techniques. Unlike results of other groups, we do not see any SiH_2 bonds upon addition of Ge to a-Si:H, thus confirming that our films are different from other glow-discharge generated a-(Si,Ge):H films. We believe this difference may be due to the different plasma environment during growth of our films. The absence of SiH_2 and other polymer bonds may also explain why our photo-to-dark conductivity ratios are so much higher than those of other groups.

1.2 NON-SEMICONDUCTOR RESEARCH

We have initiated experimentation to develop a 2-level, stable back contact to a-Si:H. Preliminary results indicate that a Cr/Pd contact may be stable and moderately reflecting. The best reflection is still obtained with Ag.

We have looked at alternatives to Al as a contact to SnO_2, in view of the reactivity of Al with SnO_2. We find Mo is a suitable, stable contact to SnO_2.

We have initiated a program to compare the adequacy of different SnO_2 substrates by growing devices in the same run on different substrates. Our results indicate that CVD SnO_2 has less absorption in the short wavelength range than spray-pyrolysis SnO_2.

1.3 SINGLE-JUNCTION DEVICE RESEARCH

We have grown a-Si:H devices with an efficiency of 8.5% in the multi-sector reactor. A critical parameter in achieving high efficiency is plasma-cleaning between deposition of the p- and i-layers.

We have grown a-(Si,Ge):H devices with an efficiency of 6.5%. These devices were grown in the single-chamber reactor.

We have studied the influence of the aging of ELH lamps on the spectral characteristics of these lamps and, hence, on apparent efficiency of a-Si:H devices. We find that a variation in the spectral content of ELH lamps can impact the accuracy of the efficiency measurement. We now routinely measure our efficiency by true outdoor measurements and also check it by comparing measured current with current calculated from QE measurements.

We have made a study of the use of c-Si reference cells with a cut-off filter for setting simulator intensity. We find that this method is prone to severely under-estimate the efficiency of good a-Si:H cells with a high QE in the 700 nm range, and is even more unsuitable for tandem cell measurements.

1.4 TANDEM-JUNCTION DEVICE RESEARCH

We have made two types of tandem cells: high-gap/medium-gap (a-Si:H/a-Si:H) cells and high gap/low gap (a-Si:H/a-(Si,Ge):H) cells. We have achieved efficiency of 7.4% in the first type of cell, and 6.7% in the second type of cell. These efficiencies were measured using both a Spectrolab Xenon X-25 simulator, and outside sunlight at 100-105 mW/cm^2.

SECTION 2
MATERIAL GROWTH

2.1 MATERIAL GROWTH OF a-Si:H IN MULTI-SECTOR REACTOR

The 6-sector, load-locked rotary reactor, which has been described in a previous report,[1] was utilized to grow a-Si:H films and devices. It will be recalled from our previous work[2] that we had found that plasma cleaning of our single-chamber reactor had a large influence on improving material quality. Based on that result, we expected that growth in our multi-sector reactor, which is equipped with both load-lock and plasma cleaning, should lead to films with even higher quality than previously reported. In Table 2-1, we show the comparative photo and dark conductivities that we obtain in the single and multi-sector reactors. Quite clearly, the significantly lower dark conductivity and the higher photo-to-dark conductivity ratios[3] in films grown in the multi-sector reactor indicate that these films are inherently better than films grown in the single-chamber.

TABLE 2-1. PROPERTIES OF a-Si:H

	σ_D(S-cm^{-1})	σ_{PC}(S-cm^{-1})	Ratio
Multi-chamber Reactor	7.9×10^{-11}	1.4×10^{-4}	1.8×10^{6}
Single-chamber Reactor	2.1×10^{-10}	9.4×10^{-5}	4.4×10^{5}

2.2 INFLUENCE OF H_2 DILUTION OF SiH_4 ON FILM PROPERTIES

It has been known for some time that H_2 dilution of SiH_4 in the gas phase has some influence on the bandgap of the films.[4] We have used this information to modify both the bandgap of a-Si:H films, and, more surprisingly, to reduce the disorder due to valence band tail states.[5]

We find that diluting SiH_4 with H_2 increases the bandgap of a-Si:H to about 1.85 eV, compared to the normal 1.78 eV without H_2, for films grown at a substrate temperature of ~250°C. In Figure 2-1, we show a typical absorption curve for a film grown in the multisector reactor. We have also measured the inverse slope E_o of valence band tail-states as a consequence of H_2 dilution. It will be recalled from a previous report[1] that valence band tail-states typically follow a relationship $N_v = N_{vo} \exp(-\Delta E/E_o)$, where ΔE is the difference in energy between valence band and a particular midgap energy, and E_o is a characteristic fall-off energy. The characteristic energy E_o is a measure of disorder in the material.[5] The higher the E_o, the poorer the material.[5]

In our previous report,[1] we showed that sub-bandgap quantum efficiency (QE) measurements on devices can be used to estimate E_o. Using this technique, we find that E_o for films grown with H_2 dilution in the gas phase is about 3-5 meV smaller than for films grown without H_2 dilution. In Figure 2-2, we plot log QE vs. photon energy for two a-Si:H films, one with H_2 dilution, and one without. Quite clearly, the film with H_2 dilution has a smaller E_o (sharper curve) than the one without.

We find a similar result for a-(Si,Ge):H films. In Figure 2-3, we plot log QE vs. photon energy plots for two typical a-(Si,Ge):H films with $E_g \sim 1.55$ eV. Once again, E_o is smaller for films with H_2 dilution than for films without.

While we do not understand these results completely, we believe the basic physical mechanism is that the presence of excess H in the gas plasma may lead to etching of a-Si:H during growth.[6] During etching primarily the valence band is being lowered.[7] A consequence of this etching during growth may be a reduction in the number of defect states which are far away from the valence band edge, and therefore can be expected to have the lowest bond energy. Thus, H_2 may both push the valence band down, and etch away some weak states.

These results are significant from a device viewpoint. The increase in E_g is advantageous from a tandem-junction viewpoint, since the first cell needs a E_g of $\sim$1.85 - 1.90 eV for high tandem cell efficiency.[8] The decrease in E_o is advantageous from the viewpoint of recombination, since fewer valence band-related defects in the mid-gap region lead to an increase in lifetime, and, hence, in V_{oc}.[9]

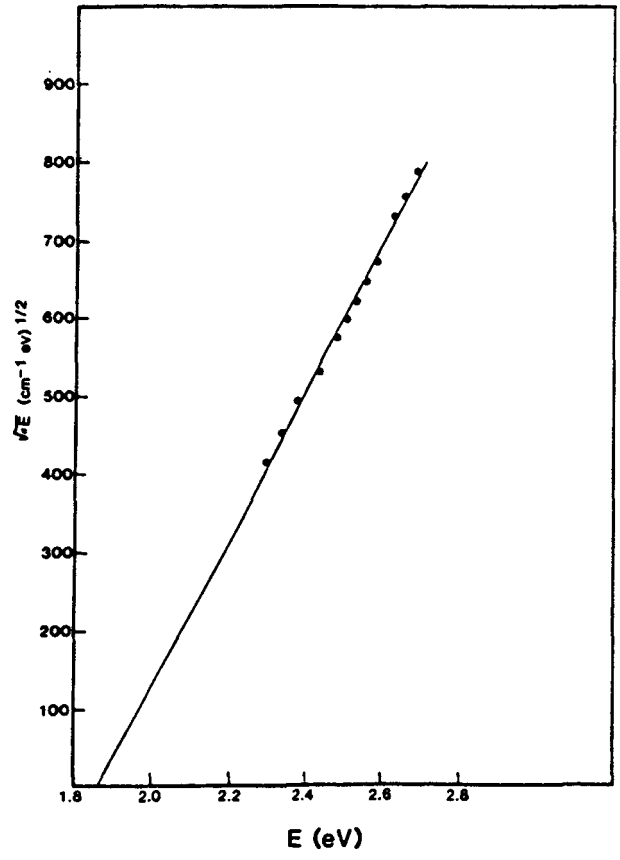

FIGURE 2-1. ABSORPTION COEFFICIENTS FOR a-Si DEPOSITED IN MULTI-SECTOR REACTOR.

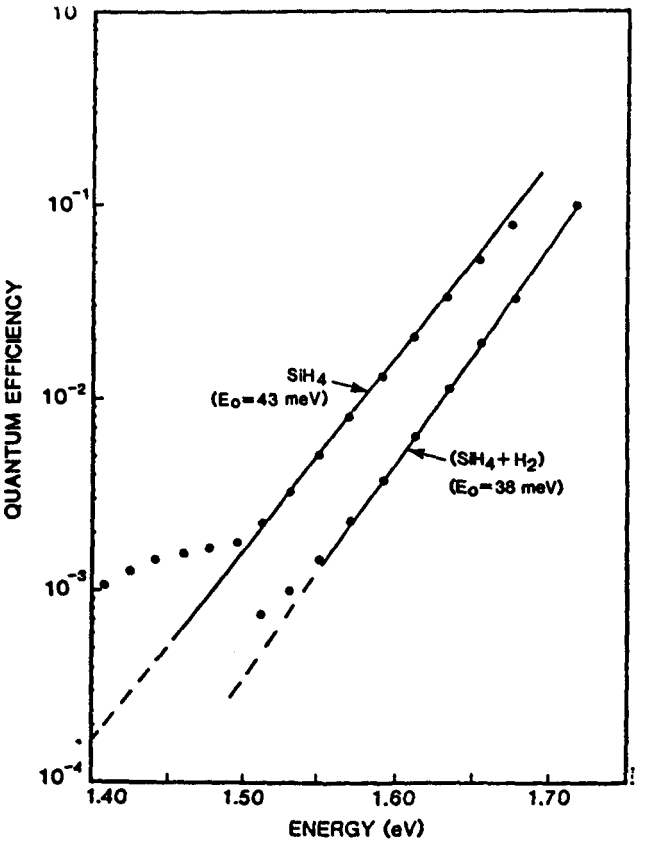

FIGURE 2-2. VALENCE BAND TAIL STATES IN a-Si FILMS.

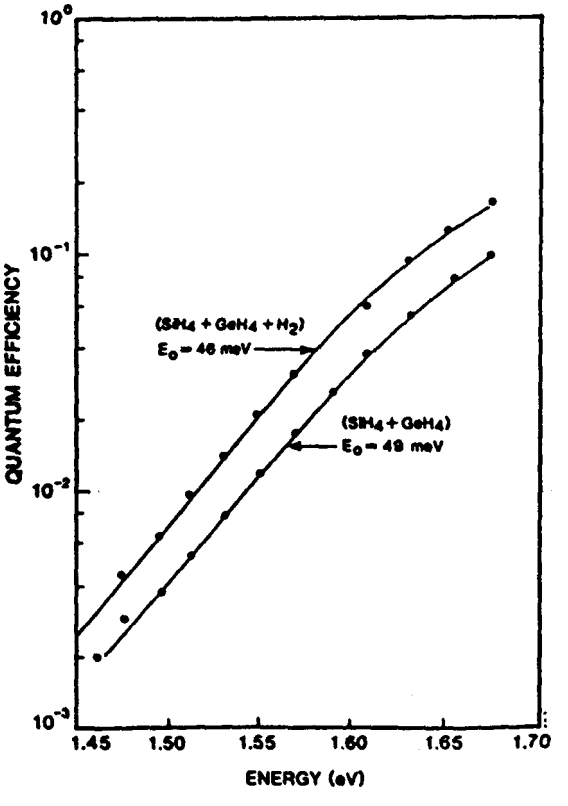

FIGURE 2-3. VALENCE BAND TAIL STATES IN a-(Si-Ge) FILMS.

Another potential advantage of H_2 dilution of SiH_4 and GeH_4 may be in allowing tailoring the bandgap of a device. If indeed the valence band is moving down as E_g increases, with the energetic position of the conduction band remaining virtually unchanged, then it becomes possible to add an electric field assist to holes in the valence band by grading the bandgap during the growth of the i-layer. Grading the bandgap in appropriate regions of the device by ~ 0.1 eV can provide a field assist of $2\text{-}5 \times 10^3$ V/cm, or an increase in the range ($\mu\tau E$) of holes of ~ 0.8 to 2.0 μm, thus doubling the collection length. Appropriate grading can thus increase the collection efficiency of holes, and allow higher fill factors and currents. Figure 2-4 illustrates this concept by showing a band diagram of such a band-gap tailored device.

2.3 GROWTH AND PROPERTIES OF a-(Si,Ge):H FILMS

We have continued our work on a-(Si,Ge):H films. A technical talk was presented at the Materials Research Society meeting in San Francisco on April 17, 1985. A copy of the manuscript, which includes details of film growth and material properties, is included as Appendix A.

2.4 H BONDING IN a-(Si,Ge):H FILMS

It has been observed by some groups [10,11] that the a-(Si,Ge):H films produced by a diode glow discharge from $SiH_4$and GeH_4 tend to have excessive SiH_2 bonding, even under conditions when no SiH_2 bonds can be expected if GeH_4 were not present. Lucovsky et. al.[11] have speculated that this peculiar phenomenon is due to the formation of higher order polymers involving SiH_4 and GeH_4 (e.g. $SiGeH_6$ etc.) in the plasma, and a consequent deposition of films from these higher order polymers, with consequent higher order Si and Ge bonds with H. Lucovsky et al. show that films produced from simultaneous reactive magnetron sputtering from individual targets of Si and Ge do not have such high order polymers.

We have determined the H bonding of our a-(Si,Ge):H films from IR measurements. Samples were prepared on polished c-Si wafers. All samples had a GeH_4/SiH_4 ratio of 20% in the gas phase, which typically leads to 1.55 eV films. We use a triode geometry in our RF discharge, with the plasma separated from the substrate by ~ 2 cm.[2] We show the results in Figures 2-5 to 2-8, for 4 films, deposited at 250° and 300°C. Quite clearly, from Figures 2-5 to 2-8, we do not see any SiH_2 bonding which would give an absorption at 2100 cm^{-1}, at least for films with Eg $\sim$1.55 eV. We believe that these results are very interesting, and are consistent with the fact that our glow-discharge films have higher σ_{pc}/σ_D ratios, compared to films made by other groups.[12] Our σ_{pc}/σ_D ratios are in the range of 1×10^5 or greater, whereas the Mitsubishi group[12] reports ratios of $\sim 10^4$ for films of Eg$\sim$1.55 eV. We believe that our triode geometry allows an effective separation between polymerization and deposition, and the fact that we can control the bias of our substrates (generally negative) also allows control over the bonding of H.[13]

Further work on H bonding will continue during the next semester, with films of different (Si,Ge) content, and grown under different conditions.

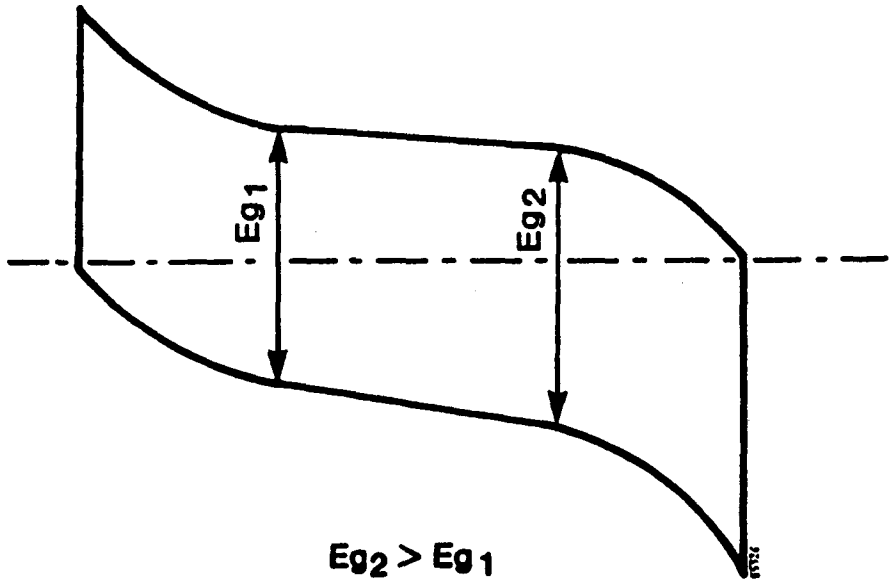

FIGURE 2-4. GRADING OF BANDGAP IN i-LAYER.

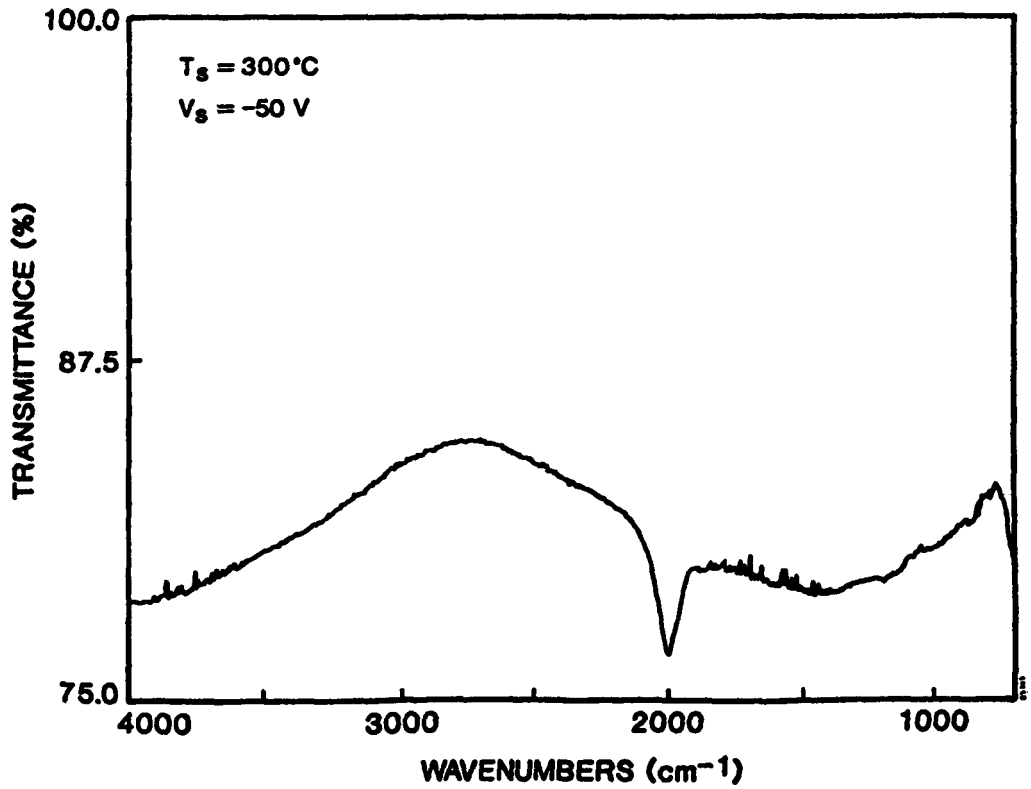

FIGURE 2-5. IR ABSORPTION IN a-(Si,Ge):H, T_S = 300°C, V_S = -50V.

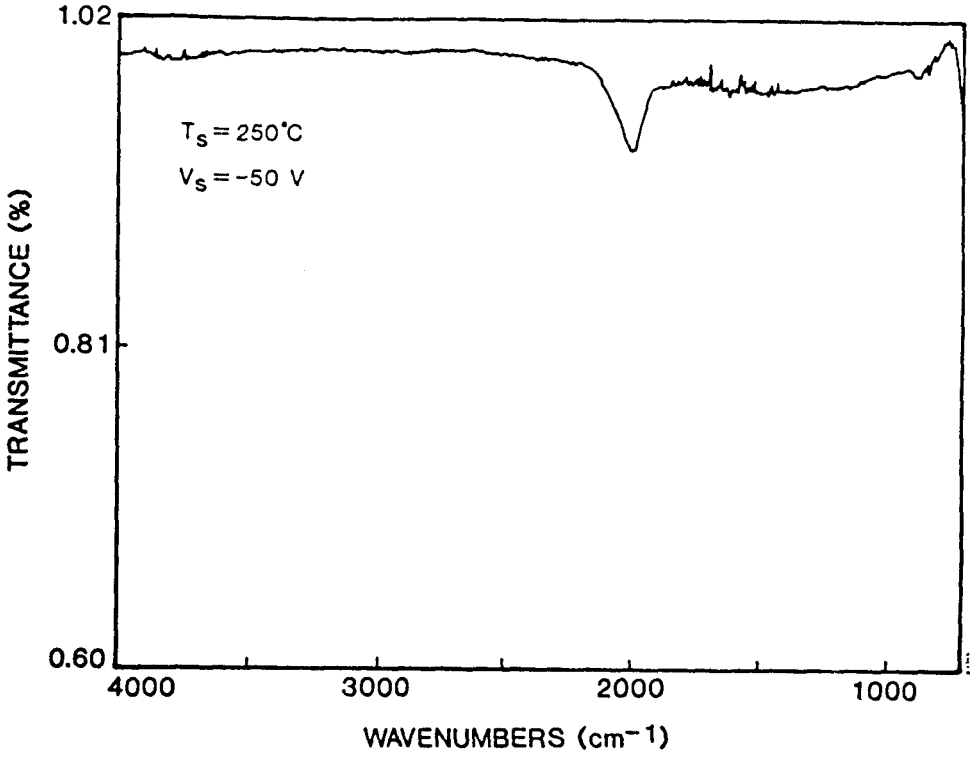

FIGURE 2-6. IR ABSORPTION IN a-(Si,Ge):H, T_S = 250°C, V_S = -50V.

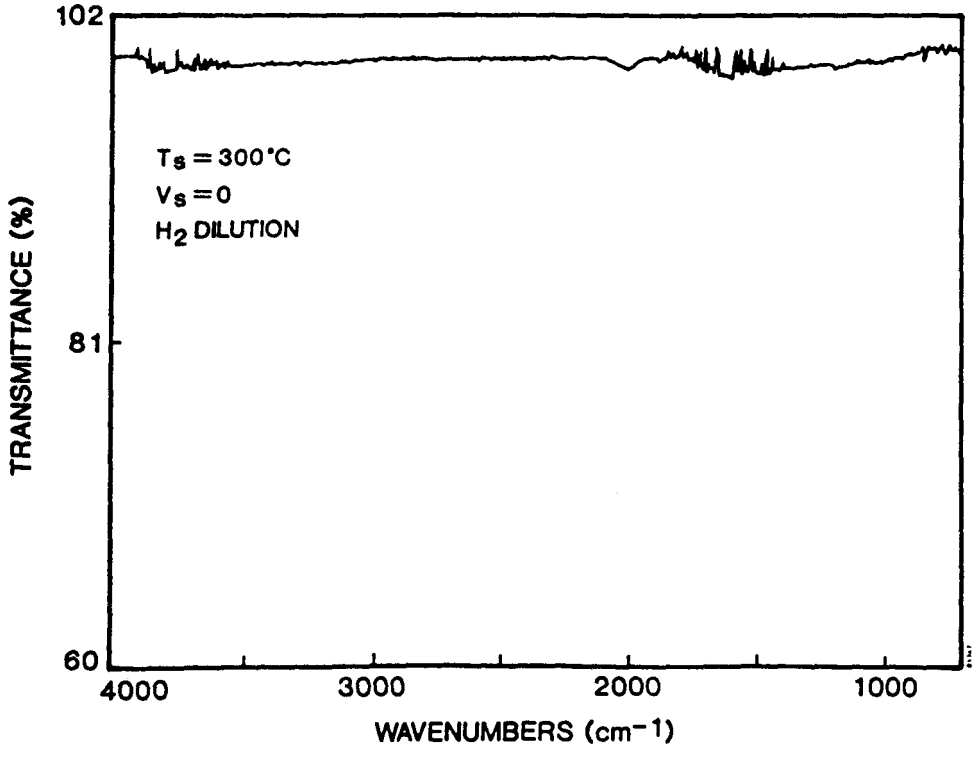

FIGURE 2-7. IR ABSORPTION IN a-(Si,Ge):H, T_S = 300°C, V_S = 0, H_2 DILUTION OF GAS MIXTURE.

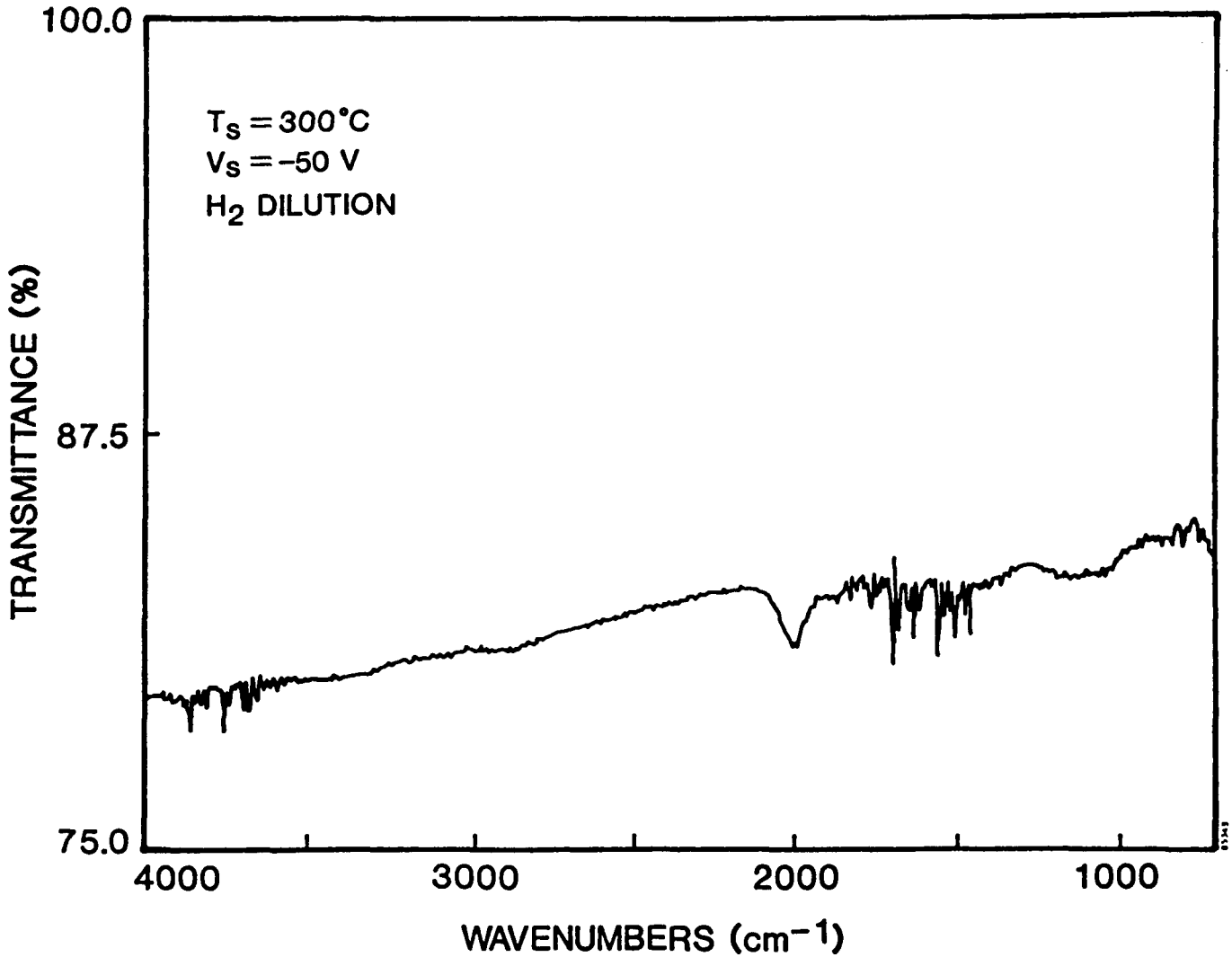

FIGURE 2-8. IR ABSORPTION IN a-(Si,Ge):H, T_S = 300°C, V_S = -50 V, H_2 DILUTION.

SECTION 3
NON-SEMICONDUCTOR RESEARCH

3.1 INVESTIGATION OF HARVARD CVD SnO_2 SUBSTRATES.

We have been working with Professor Roy Gordon's group at Harvard to investigate the use of high conductivity CVD SnO_2 made by his group as substrates for a-Si cells. The typical absorption spectra, for Harvard SnO_2 are shown in Figure 3-1. There is some (18%) absorption loss at 400 nm, but it is smaller than in similar Cherry Display spray-pyrolysis SnO_2, see Figure 3-1. We have made a-Si:H cells on Harvard SnO_2, and the typical results are shown in Figure 3-2. The cell efficiency is quite good. The corresponding QE is shown in Figure 3-3. It will be observed from Figure 3-3 that the QE in the blue region is quite good, but at 700 nm, QE is only 18%, compared to about 30% for cells prepared on Cherry Display SnO_2 (Figure 3-4). Quite clearly, then, at the present time, Harvard SnO_2 is not sufficiently textured to give high QE in the red region of the spectrum.

3.2 INVESTIGATION OF DIFFERENT METAL CONTACTS.

We have investigated 3 different metal systems as suitable back contacts for a-Si:H. The characteristics that a metal contact should have are: high reflectivity and stability against diffusion or alloying. The three metals investigated are: Al, Pd and Ag. Of these we find that Ag has the best reflectivity and is least stable, Al is the next best reflector, and is reasonably stable, and Pd is the most stable,[14] but the least reflecting. All 3 give ohmic contacts in contact with n+ a-Si:H.

In Figure 3-5 and 3-6, we show QE curves for a-Si:H cells with Ag, Al and Pd contacts. For comparison, we evaporated Ag and Al on one device, and Al and Pd on another device, thus using Al as a control. The results from Figure 3-5 and 3-6 show that QE in the red is enhanced most for Ag, and least for Pd, thereby leading us to believe that Ag is the best contact for a-Si from a reflection viewpoint.

During the next period, we will investigate Cr/Ag and ITO/Ag bilayer contacts to see if a stable contact can be achieved.

3.3 INVESTIGATION OF ALTERNATIVE CONTACTS TO SnO_2

It has been reported previously[15] that Al contacts to SnO_2 may be prone to degradation due to formation of Al_2O_3. Therefore, as an alternative, we have investigated the use of Mo as a contact to SnO_2. Typically, strips of Mo are put down on SnO_2, and then a-Si devices are deposited through a mask onto uncoated portions of SnO_2. Standard Al back contacts are made to n^+ layers of a-Si.

We find that indeed, Mo-SnO_2 contacts are very stable and do not degrade over time. Further work to study contact resistance etc. will be done during the next semester.

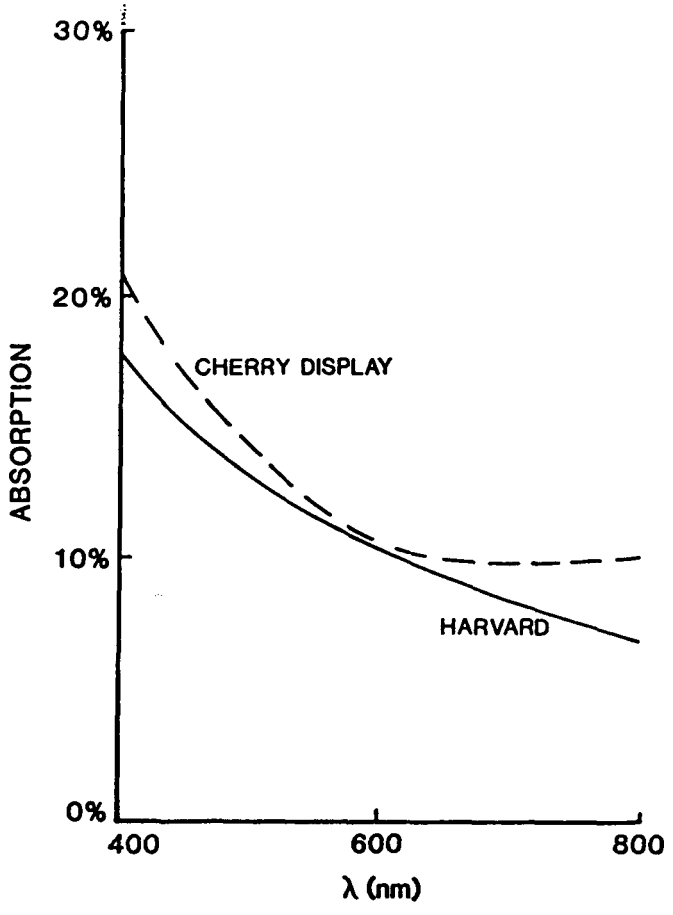

FIGURE 3-1. ABSORPTION OF HARVARD AND CHERRY SnO_2 FILM.

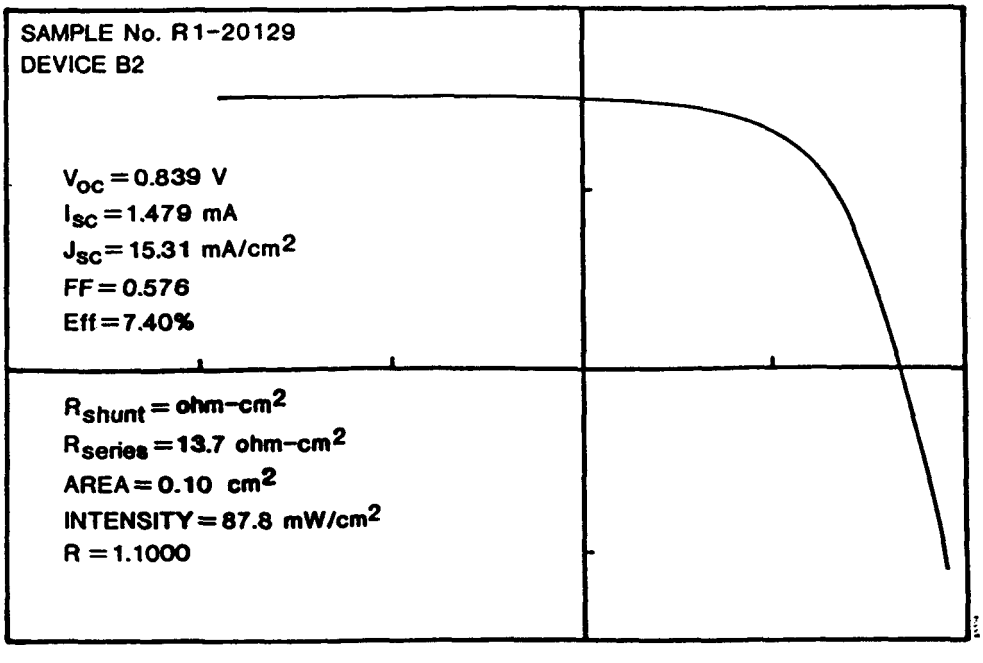

FIGURE 3-2. I(v) CHARACTERISTICS OF a-Si:H CELLS ON HARVARD SnO_2 FILM.

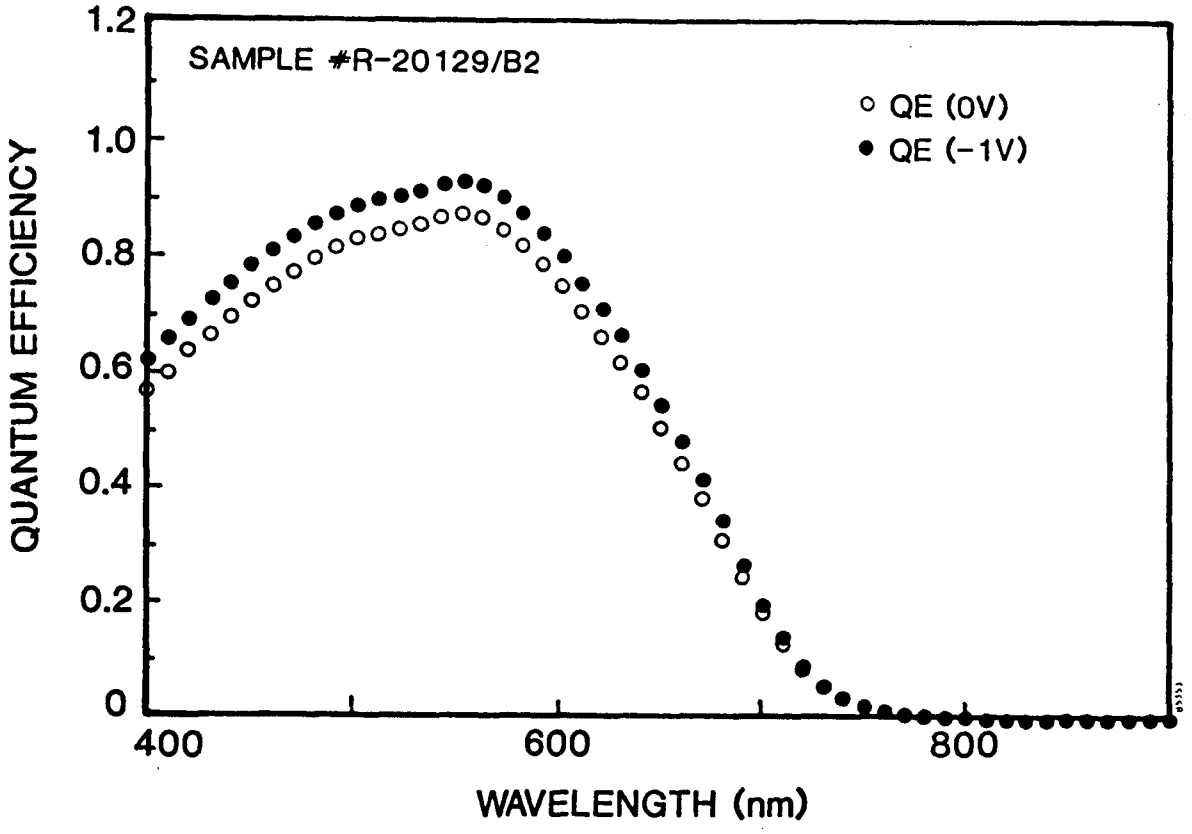

FIGURE 3-3. QE OF a-Si:H CELL ON HARVARD SnO_2 FILM.

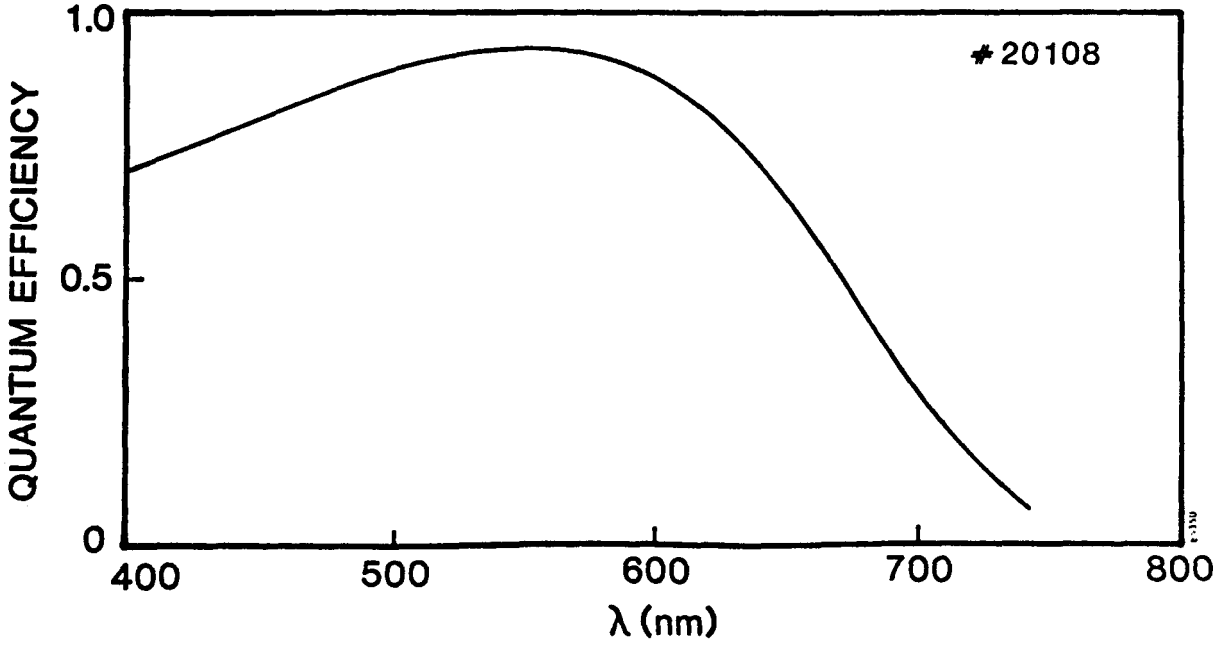

FIGURE 3-4. QE (at V=0) of a-Si:H CELL ON CHERRY DISPLAY SnO_2.

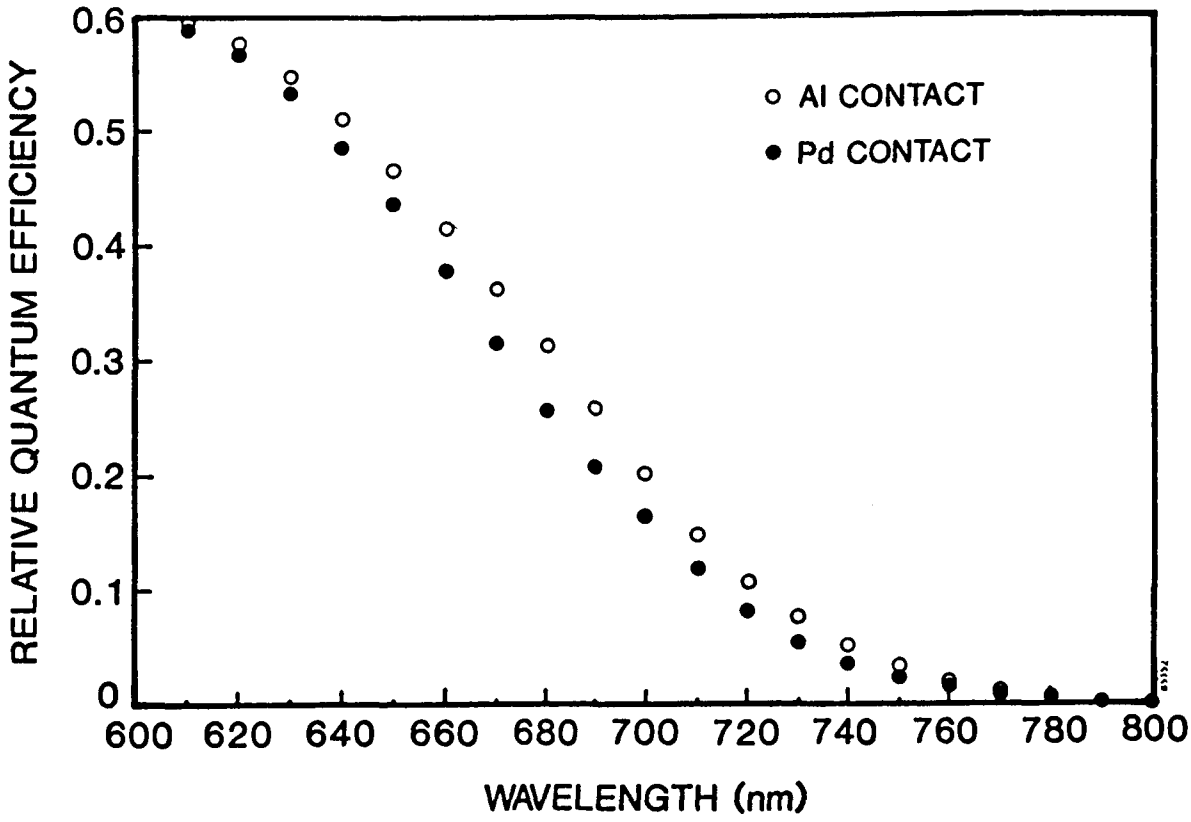

FIGURE 3-5. COMPARISON OF QE for a-Si:H CELLS WITH Al and Pd BACK CONTACTS

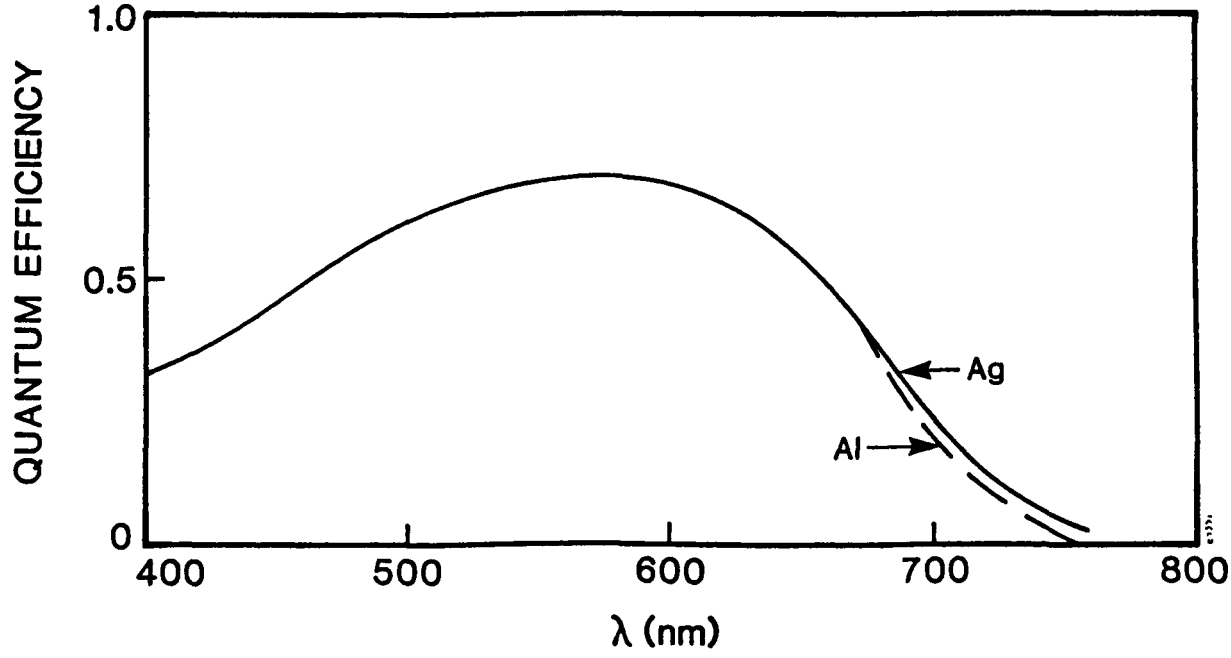

FIGURE 3-6. COMPARISON OF QE FOR a-Si:H CELLS WITH Al and Ag BACK CONTACTS

SECTION 4
SINGLE JUNCTION CELL RESEARCH

4.1 RESEARCH ON a-Si:H SOLAR CELLS

We have continued our work on improving efficiency of single-junction a-Si:H solar cells. Much of this work has concentrated on three areas.

i) Device growth in multi-sector reactor.

ii) Use of graded bandgap layers to control electron back-diffusion.

iii) Careful calibration techniques for solar cell measurements.

4.2 DEVICE GROWTH IN MULTI-SECTOR RECTOR

It will be recalled[1] that the multi-sector reactor allows growth of p-, i- and n-layers in separate sectors, with provision for plasma cleaning of each sector between the growth of different layers.

We have grown p-i-n cells in the multi-sector reactor with and without plasma-cleaning between p- and i-layers. It is well known that B_2H_6, which is used for growing p-layers, tends to adsorb on the walls of the reactor and to desorb during growth of the subsequent i-layer, thereby contaminating the i-layer.[16] Therefore, in the absence of a plasma cleaning of the reactor, we would expect a B contamination of the i-layer even in the multi-sector reactor. On the other hand, plasma cleaning before i layer growth should lead to a coating of a-Si:H on the walls, which should bind up any residual B_2H_6 into the wall coating, and minimize B incorporation into the device. Since the different sectors are not gas-isolated, B_2H_6 would be absorbed onto the walls of all the sectors, and therefore, the best cleaning would be expected to be a plasma cleaning of all 6 sectors. This is exactly what we find in practice.[8]

In Figures 4-1 to 4-4, we show the results of the plasma-cleaning experiments. In Figure 4-1, we plot the I(V) curve for a p-i-n sample deposited on SnO_2 glass in 3 sectors without any plasma cleaning between p- and i-layers. In Figure 4-2, we plot the corresponding ratio of QE(-1V)/QE(0V) vs. wavelength. (It will be recalled from our previous report[1] that this ratio is a sensitive indicator of B contamination at p-i interface. A high ratio (>1.5) indicates severe contamination.) Upon examining Figure 4-1 and 4-2, we note that the I(V) curve has a high series resistance in forward bias (16.5 ohm-cm^2), and the current keeps increasing in reverse bias, both indications of B contamination. The QE data (Figure 4-2) is quite convincing. The very high ratio QE(-1V)/QE(0V) for λ = 400 nm, and the monotonic decrease in this ratio with increasing λ, are a clear indication of a low electric field at p-i interface,[1] i.e. p-type contamination of the i-layer.

In contrast, in Figure 4-3 and 4-4, we plot the results for a sample where a cleaning plasma was ignited in all 6 sectors between p- and i-layers. In Figure 4-3, we see a normal I(V) curve, with a lower series resistance (13.0 ohm-cm^2) than the B-contaminated cell and a flat I under reverse bias. The QE ratio data in Figure 4-4 shows a very low QE ratio (1.1) at 400 nm, decreasing to 1.07 at 600 nm and increasing to 1.15 at 800 nm, characteristics of a high electric field at the p-i interface, and limitation coming from hole ($\mu\tau$) products at long wavelengths.[1]

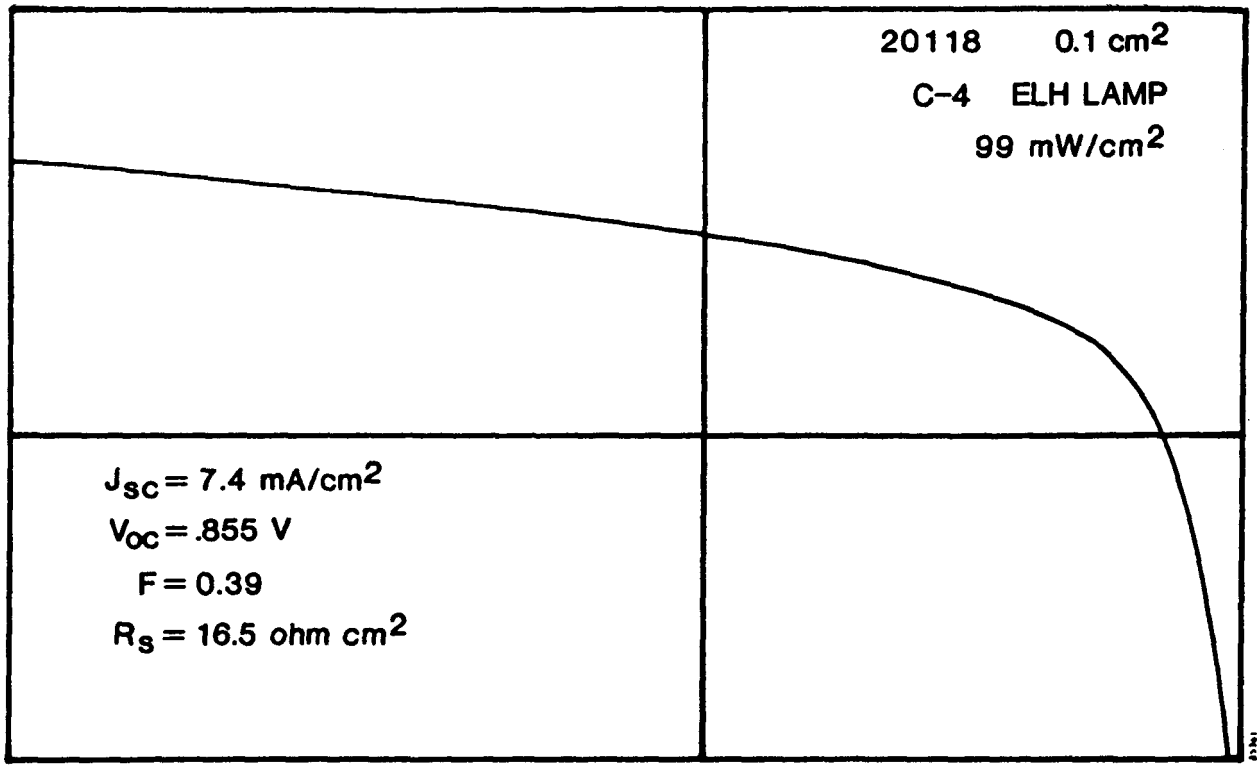

FIGURE 4-1. I(V) CURVE OF a-Si:H CELL WITH B CONTAMINATION.

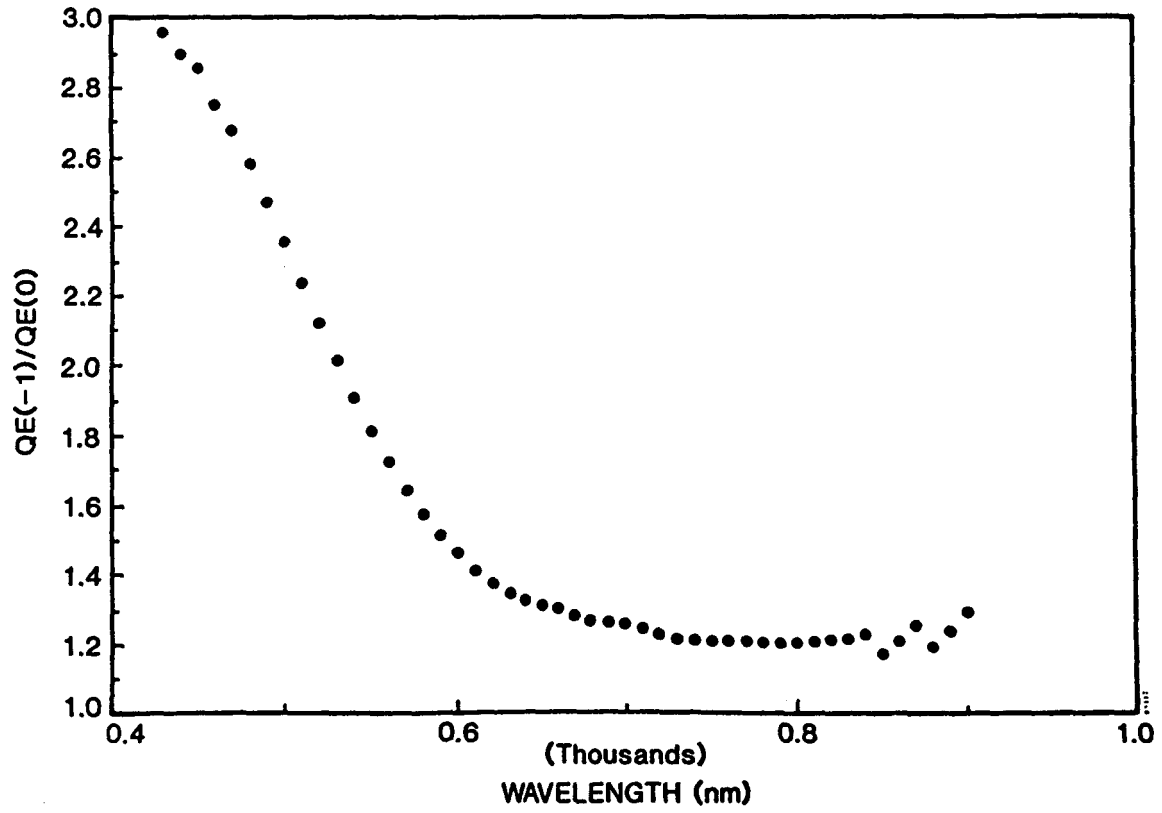

FIGURE 4-2. QE OF CELL SHOWN IN FIGURE 4-1.

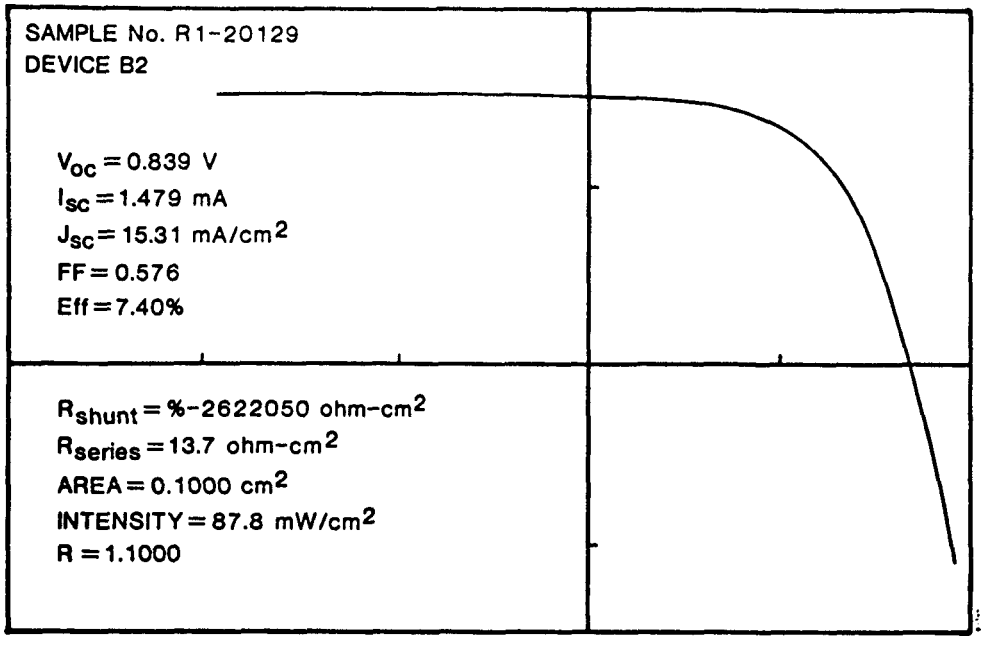

FIGURE 4-3. I(V) CURVE OF a-Si:H CELL WITHOUT B CONTAMINATION.

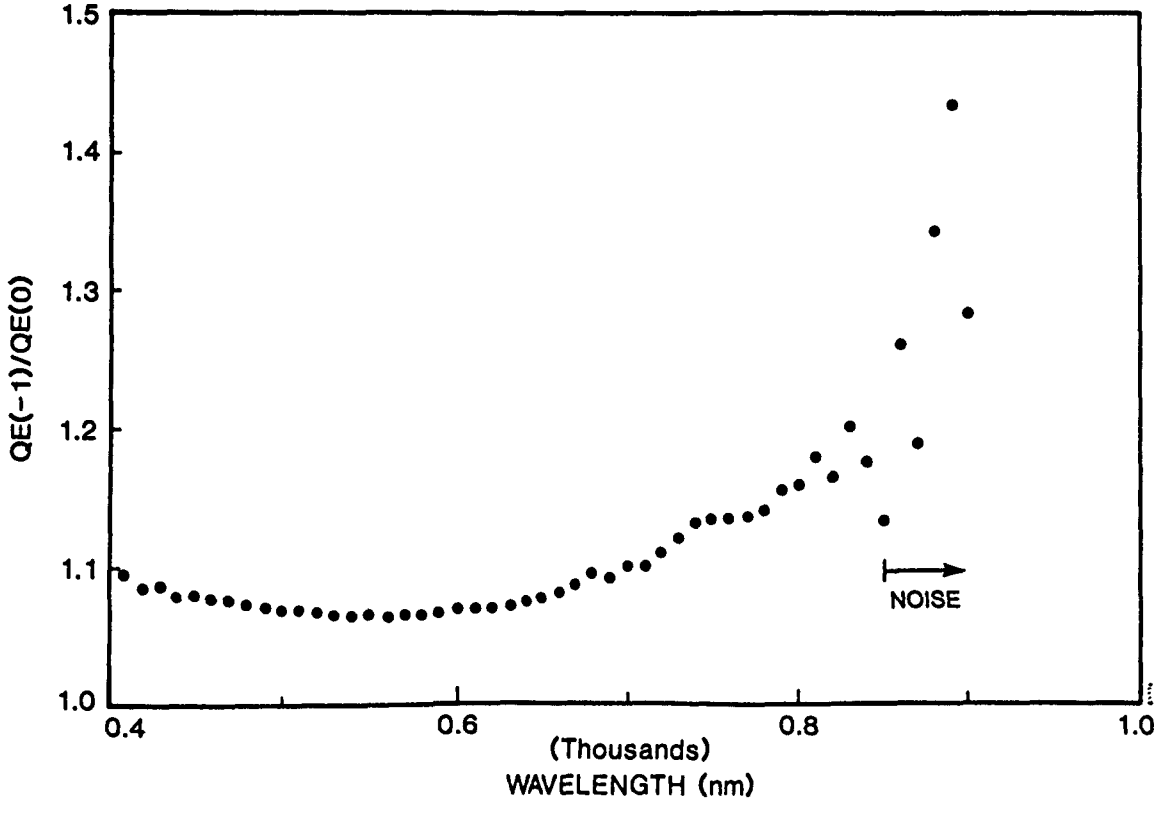

FIGURE 4-4. QE RATIO OF CELL SHOWN IN FIGURE 4-3.

Quite clearly, then, plasma cleaning with a SiH_4 plasma in each sector is very important for achieving sharp interfaces and minimum cross-contamination, a result consistent with our earlier observations on i-layers produced in the single-sector reactor.[2]

Using similar plasma cleaning techniques, and control over p-layer thicknesses, we have achieved 8.4-8.5% efficient devices in the multi-sector reactor. Figure 4-5 shows a typical I(V) curve for an 8+% a-Si:H device. The measurement techniques are described in detail in a later section. Typical parameters for growing p-i-n devices are listed in Table 4-1.

4.3 USE OF GRADED BANDGAP i-LAYER TO CONTROL ELECTRIC FIELD AT p-i INTERFACE

It was suggested by Wiedeman and Fagen[17] that a bandgap grading of the conduction band in the i-layer away from the p-i interface will lead to a decrease in back-diffusion of electrons from the i-layer to the p-layer. Figure 4-6 illustrates this concept.

We have been doing such bandgap grading of i-layers by varying the C:Si ratio in the i-layer over the first few hundred Angstrom units. We find a dramatic influence of such grading on devices produced in the single-chamber reactor, where, presumably, residual B contamination of the i-layer near the p-i interface can be counteracted by the electric field provided by the grading of the conduction band.

In Figure 4-7, we show the reverse bias QE ratio vs. wavelength with and without conduction band grading. From Figure 4-7, we see that grading of the conduction band in a single-chamber reactor leads to a smaller QE ratio at λ =400 nm, an indication that electron back diffusion is reduced.[1]

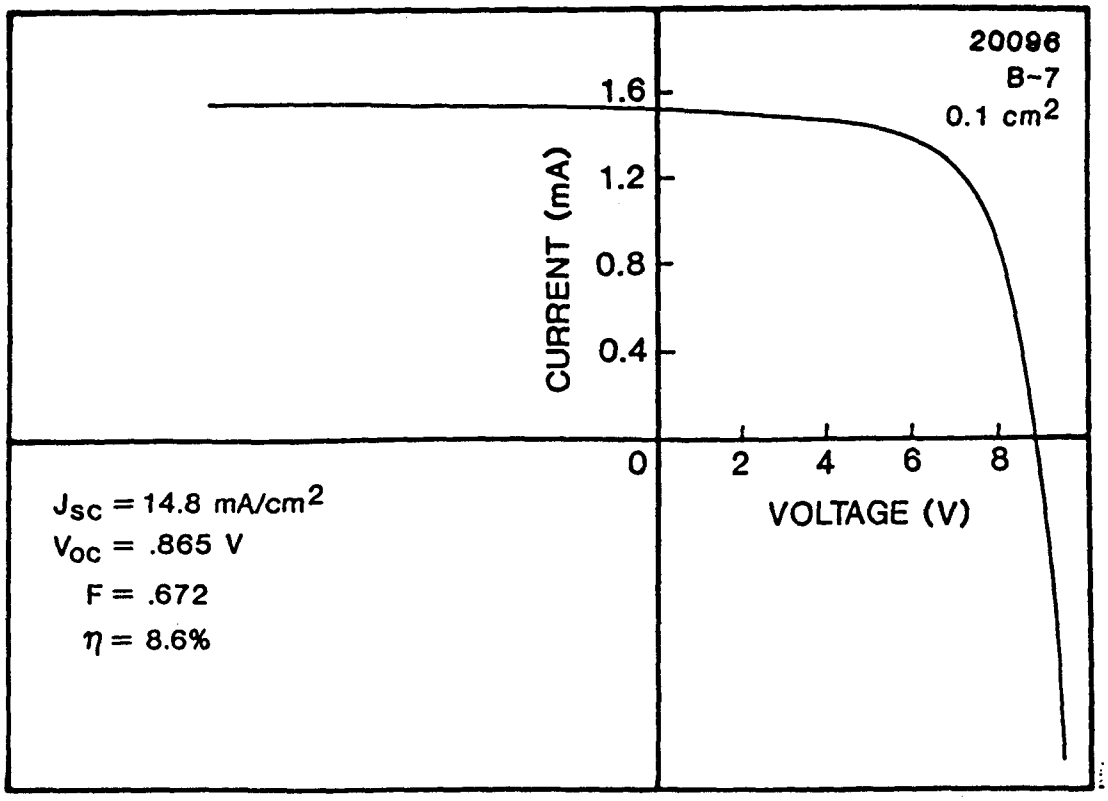

FIGURE 4-5. I(V) CURVE OF AN 8.6% CELL.

TABLE 4.1 DEPOSITION PARAMETERS FOR a-Si:H (20096)

1. p+ layer: Eg = 1.9-0 2.0 eV
   t = 100-200 Å (estimate)
   $B_2H_6/(SiH_4 + CH_4)$ = 0.5%
   p = 200 μm Hg
   T = 220°C

2. Plasma cleaning between p and i layers

3. i layer:
   Eg = 1.82 eV
   t = 0.7 μm Hg
   SiH_4/H_2 = 1/3
   p = 200 μm
   T = 250°C
   $V_{substrate}$ = -10V
   Power = 35 mW/cm^2
   Deposition Rate = 1-2 Å/sec.

4. n+ layer:
   Eg = 1.75 eV
   PH_3/SiH_4 = 2.0%
   T = 300°C
   p = 200 μm Hg
   t = 500 -1000 Å (estimate)

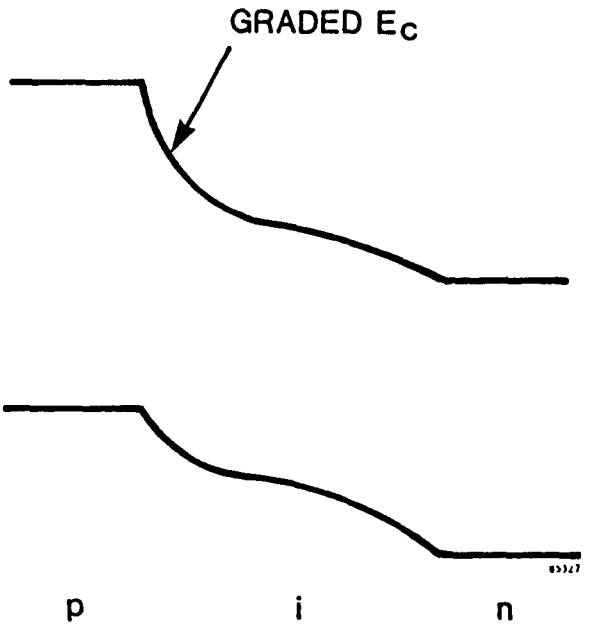

FIGURE 4-6. GRADED CONDUCTION BAND IN i-LAYER AT p-i INTERFACE.

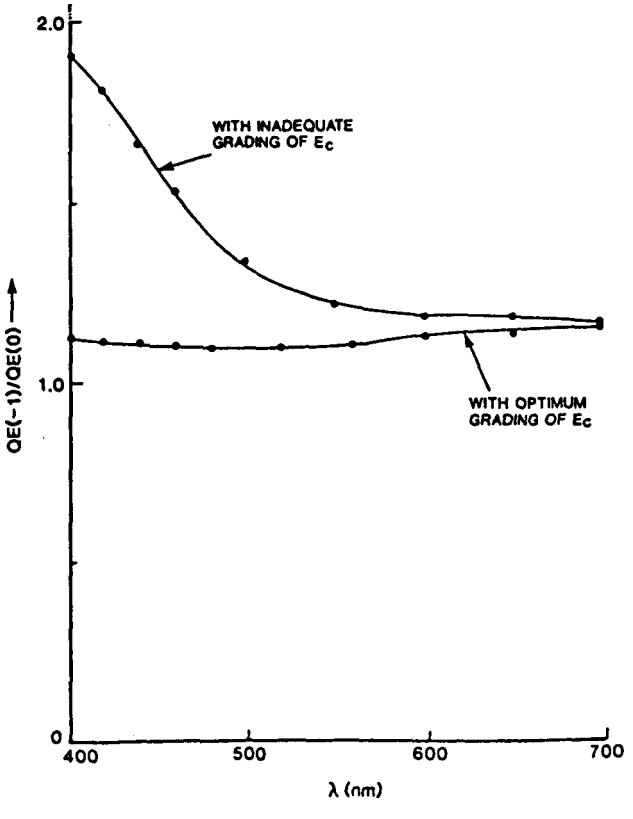

FIGURE 4-7. QE RATIO OF a-Si:H CELLS PRODUCED IN THE SINGLE-CHAMBER REACTOR WITH AND WITHOUT CONDUCTION BAND GRADING.

4.4 CALIBRATION OF EFFICIENCY MEASUREMENTS

An important aspect of any cell efficiency measurement is the calibration techniques used to verify efficiency. This subject is sufficiently important to deserve a detailed discussion, which is attached as Appendix B.

4.5 RESEARCH ON a-(Si,Ge):H CELLS

During the previous semester, we demonstrated that we can make p-i-n a-(Si,Ge):H cells. During this semester, we have improved the performance of p-i-n cells to 6.5% efficiency.

The first question in the design of a-(Si,Ge):H cells is what kind of p-layer to use. It will be recalled from our previous report[1] that the problem of electron affinity match between a wide bandgap p-layer and the i layer of a-(Si,Ge):H must be addressed before an efficient p-i-n cell can be made. In particular, we are faced with two seemingly incompatible results on electron affinities. The work of Tiedje et al.[18] on a-Si:H/a-Ge:H superlattices suggest that the two valence bands are matched, and that the discontinuity is entirely at the conduction band interface. If that is so, p a-Si:H, or p a-(Si,C):H, can be a good window p-layer for a-(Si,Ge):H. On the other hand the work of Wiedeman and Fagen[17] suggests that the conduction bands of a-Si:H and a-(Si,Ge):H are matched in electron affinity, and that the discontinuity is at the valence band interface. If this latter result is correct, we cannot use p-a-Si:H, or p-a-(Si,C):H, as a window layer for i a-(Si,Ge):H, since it would lead to an energetic trap for holes at p-i interface. (These concepts were explained in our previous report[1] in detail).

We have experimented with using p a-(Si,C):H as a window layer for different a-(Si,Ge):H i-layers. All structures were p-i-n, with i- and n-layers always having the same Si:Ge ratios. Only the p-layer was a different bandgap. We expect that if there were a hole trap at the p-i interface, we would get an anomalous I(V) curve, in particular, a severe decrease in current with forward bias, as shown schematically in Figure 4-8. As the electric field decreases, one would expect a decrease in tunneling probability of holes through the hole trap, and a significant decrease in current. On the other hand, if no hole trap exists, a normal I(V) curve should result.

The experimental results for i-layers with $E_g > 1.55$ eV (Ge<20%) show mostly normal I(V) curves. A typical curve is shown in Figure 4-9. Quite clearly, then, up to about 20% Ge, one does not find a hole trap at the p-i interface, i.e., the discontinuity must be mainly in conduction band. However, when the GeH_4 ratio in the gas mixture is increased to produce materials with $E_g < 1.5$ eV, peculiar I(V) curves, of the type expected from Figure 4-8, begin to appear (see Figure 4-10), suggesting either a poorly doped n^+ layer, or a hole-trap at the p-i interface, which would both give similar I(V) curves. It is, therefore, possible that as the Ge content increases, both conduction and valence bands move. Further work to understand this result is in progress.

4.6 IMPROVED EFFICIENCY a-(Si,Ge):H CELLS

In Figure 4-11, we show the I(V) curve for a 6.5% efficiency a-(Si,Ge):H cell; p-i-n structure, with a p a-(Si,C):H window and i- and n-layers of a-(Si,Ge):H. The bandgap is ~1.6 eV. The cell was deposited on a SnO_2 substrate. In Figure 4-12, we show the I(V) curve for a 5.7% a-(Si,Ge):H cell, with $E_g \sim 1.53$ eV i-layer. Typical parameters for preparing a-(Si, Ge) p-i-n devices are listed in Table 4.2.

TABLE 4.2 PREPARATION PARAMETERS FOR a-(Si, Ge):H PIN CELLS (#1682)

1. p layer:

   Eg = 1.9-2.0 eV
   $B_2H_6/(SiH_4 + CH_4)$ = 0.75%
   t = 100 - 200 Å
   T = 230°C
   p = 200 μm Hg

2. i layer:

   Eg = 1.65 eV
   GeH_4/SiH_4 = 10%
   p = 200 μm Hg
   T = 300°C
   $V_{substrate}$ = -50V
   Power = 35 mW/cm^2
   Deposition Rate = 1.0 Å/sec.
   t = 0.5 μm

3. n^+ layer

   Eg = 1.65 eV (same as the corresponding i layer)
   $PH_3/(SiH_4 + GeH_4)$ = 2%
   T = 300°C
   t = 500 - 1000 Å
   p = 200 μm Hg

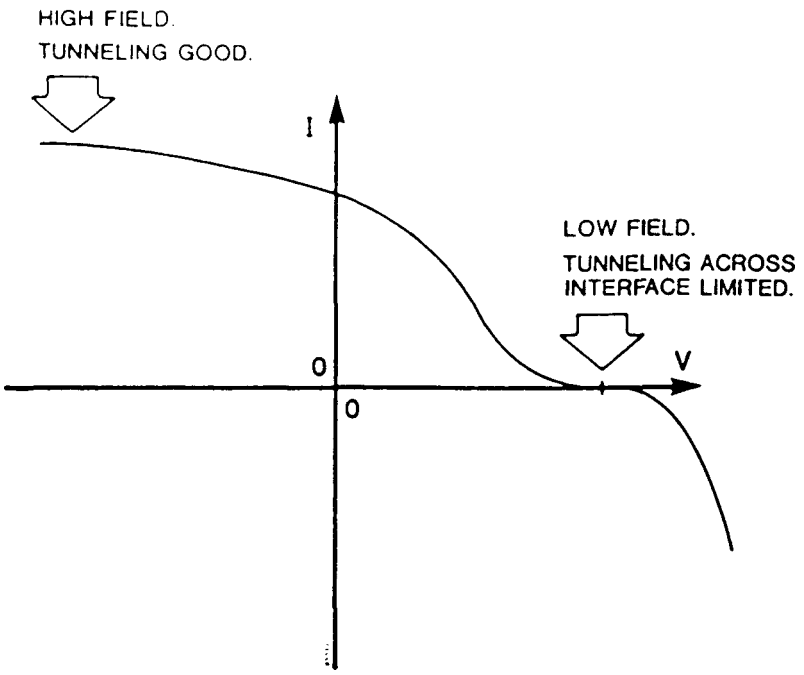

FIGURE 4-8. MODEL FOR I(V) CURVE WHEN TUNNELING INTERFACES ARE PRESENT.

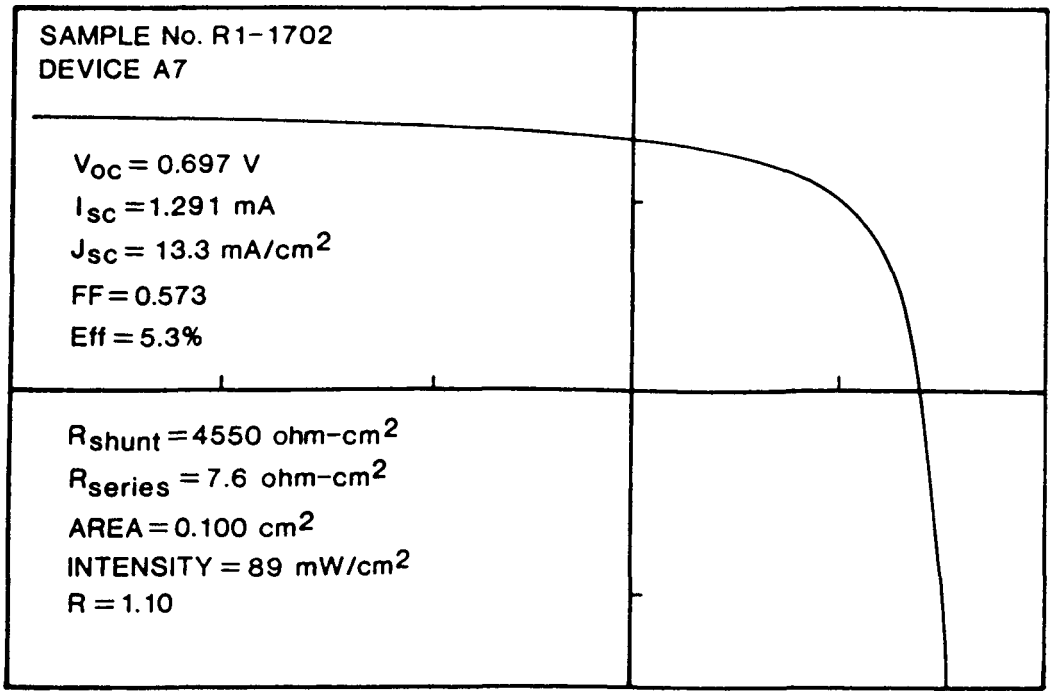

FIGURE 4-9. I(V) CURVE OF A NORMAL a-(Si,Ge) CELL.

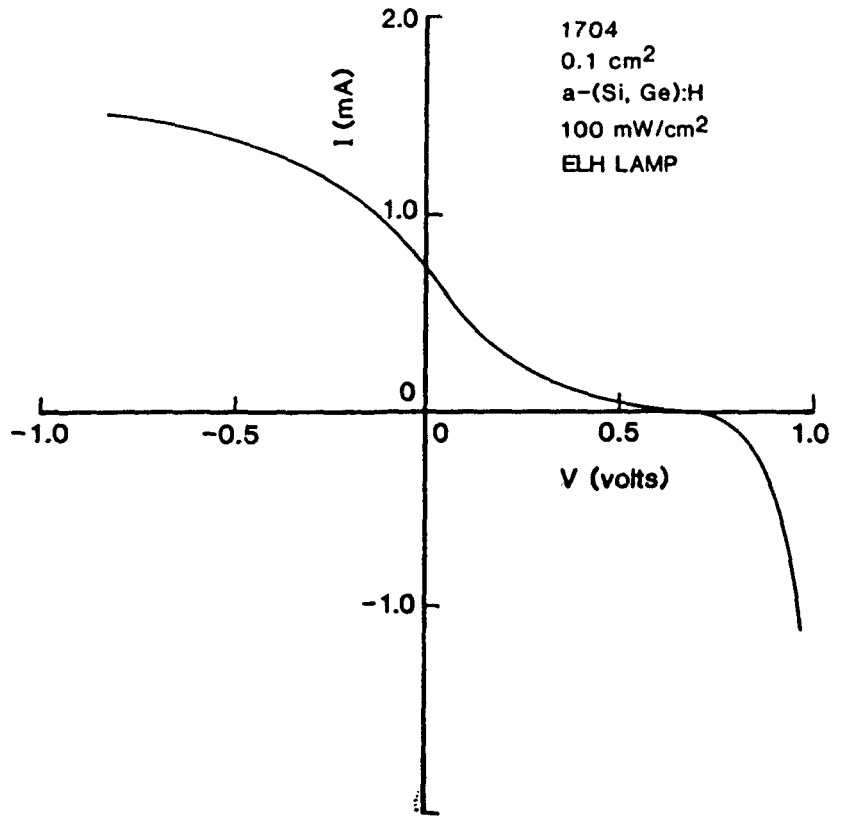

FIGURE 4-10. I(V) CURVE OF AN ABNORMAL a-(Si,Ge) CELL.

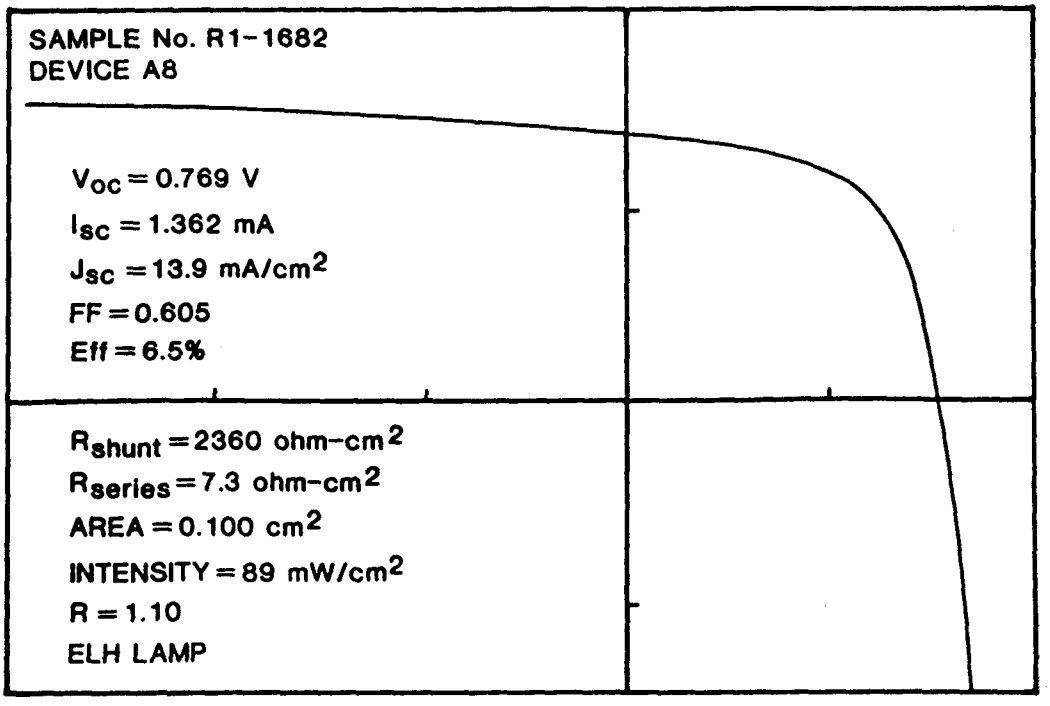

FIGURE 4-11. I(V) CURVE OF A 6.5% a-(Si,Ge) CELL.

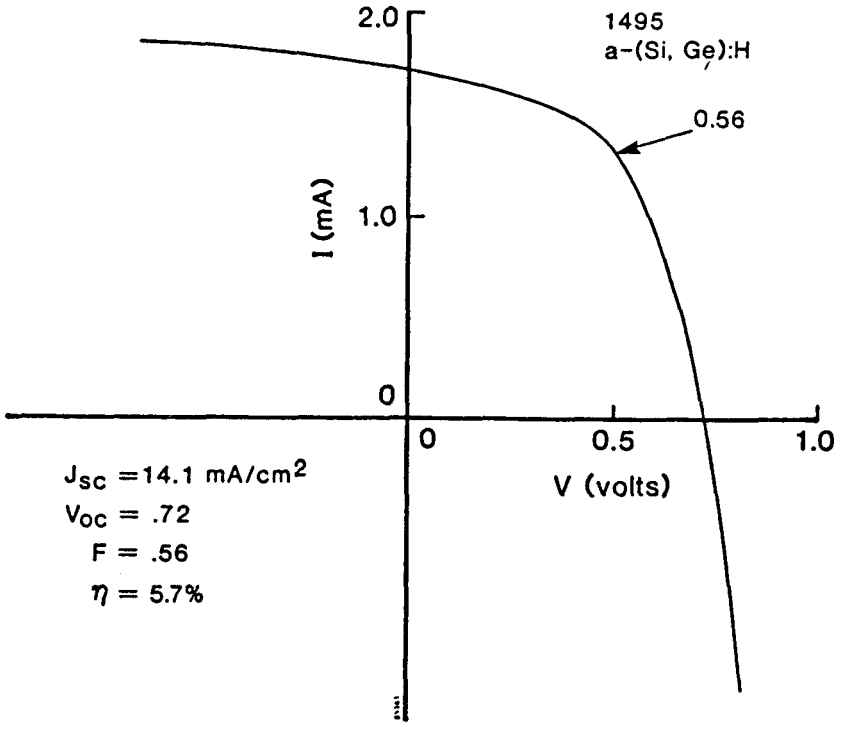

FIGURE 4-12. I(V) CURVE OF A 5.7% A-(Si,Ge) CELL.

4.7 SUMMARY OF SINGLE JUNCTION CELL RESEARCH

To summarize our work:

- The multi-sector reactor is now routinely producing standard p-i-n a-Si:H cells of >8% efficiency, with little optimization done so far.
- Moderate efficiency a-(Si,Ge):H cells have been produced in the single chamber reactor. p a-(Si,C):H appears to work well as a window material for E_g>1.55 eV.
- Future work will involve cell and material optimization, including such techniques as ppm doping of the i-layer and bandgap grading to improve hole collection.

SECTION 5

TANDEM-JUNCTION CELL RESEARCH

5.1 TANDEM JUNCTION a-Si/a-Si CELLS

We have made 7.3-7.5% efficient, high-gap a-Si/mid-gap a-Si two-junction cells. Each cell was of the p-i-n type. The typical parameters for these cells were:

1st Cell	2nd Cell
E_g = 1.85eV	E_g = 1.80 eV
t_1 = 1000Å	t_2 = 6000 Å
p_1 = a-(Si,C):H	p_2 = a-(Si,C):H
n_1 = a-Si	n_2 = a-Si

The substrate was Cherry Display SnO_2, and back contact was Al. A typical I(V) curve, measured under Xenon lamp (Spectrolab X-25), and verified with an outdoor measurement at 105 mW/cm^2 is shown in Figure 5-1. The noteworthy features are the good voltage and the excellent fill factor. The high fill factor is particularly encouraging, since it suggests that a tunnel junction between n^+ a-Si:H and p^+ a-(Si,C):H is efficient at transmitting current with little voltage loss. One would expect that the poorer doping efficiency of p-type a-(Si,C):H, compared with p a-Si:H, may inhibit tunneling. Apparently, this is not the case. The parameters for a-Si/a-Si tandem cell is shown in Table 5-1.

5.2 TANDEM JUNCTION a-Si/a-(Si,Ge) CELLS

We have made 6.7% efficient, a-Si/a-(Si,Ge) 2-junction cells (#1676). Each cell was of a p-i-n type. The structure was fabricated on Cherry SnO_2 coated glass, and had Al back contacts.

The tunnel junction was between n-type a-Si:H and p-type a-(Si,C):H. The typical layer parameters were:

1st Cell	2nd Cell
E_g = 1.82eV	E_g = 1.55 eV
t_1 = 1500Å	t_2 = 6000 Å
p_1 = a-(Si,C):H	p_2 = a-(Si,C):H
n_1 = a-Si	n_2 = a-Si

The I(V) curve is shown in Figure 5-2. The curve was measured under a Xenon lamp, and the efficiency (6.7%), as verified by an outdoor measurement at 103 mW/cm^2 was within ~3% of indoor measurements. The remarkable feature to note is the very high voltage (1.65 V). We do not understand why the voltage in this cell is higher than in the Si/Si tandem cell. The lower fill factor (0.61) is expected because of the higher series resistance of the a-(Si,Ge) layer, compared to a-Si. We wish to point out that neither the a-Si/a-Si, nor the a-Si/a-(Si,Ge) tandem cells were in any sense optimized. A systematic effort to optimize each layer, and each interface, of this cell, including better tunnel

TABLE 5-1. DEPOSITION PARAMETERS FOR a-Si/a-Si TANDEM CELL (20135)

1st Cell:

1. P layer:

   T = 250° C
   p = 200 μm Hg
   $B_2H_6/(SiH_4 + CH_4)$ = 0.4%
   Power = 30 mW/cm^2
   t = 100-200 Å (estimate)

2. I_1 layer:

   T = 275° C
   p = 100 μm Hg
   Grade Ch_4SiH_4 from 1/ 3 to 0/3 over 3 mins.

3. I_2 layer:

   T = 275→250° C
   p = 200 μm Hg
   SiH_4/H_2 = 1/4
   t = 1000-1200 Å (estimate)
   Power = 40 mW/cm^2
   $V_{substrate}$ = -10V

4. n+ layer:

   T - 275° C
   p - 200 μm Hg
   Power = 30 mW/cm^2
   PH_3/SiH_4 = 2.4%

2nd Cell:

5. p+ layer:

   T = 260° C
   p = 200 μm Hg
   Power = 30 mW/cm^2
   Eg = 1.9 - 2.0 eV
   t = 150-200 A (estimate)
   $B_2H_6/(SiH_4 + CH_4)$ = 0.4%

6. I_1 layer:

   T = 325° C
   p = 100 μm Hg
   Grade Ch_4SiH_4 from 1/ 3 to 0/3 over 3 mins.

TABLE 5-1. DEPOSITION PARAMETERS FOR
a-Si/a-Si TANDEM CELL (20135) (continued)

7. I_2 layer:

   T = 325 → 290° C
   p = 200 μm Hg
   Power = 50 mW/cm^2
   SiH_4/H_2 = 1/1.5
   $V_{substrate}$ = -10V

8. n+ layer:

   T = 325° C
   p = 200 μm Hg
   Power = 40 mW/cm^2
   t = 1000 Å (estimate)
   Ph_3/SiH_4 = 2.4 - 2.8%

junctions and graded bandgap i-layers (as discussed in Section 4), will be undertaken during the next semester. We believe that our extensive work on understanding each cell material and interface independently will pay off during the next part of the program and lead to better tandem junction devices. The parameters for a-Si/a-(Si, Ge) tandum cell is shown in Table 5-2.

5.3 MEASUREMENT TECHNIQUES FOR TANDEM JUNCTION CELLS

A reliable measurement of tandem-junction cells is extremely difficult indoors, since no simulator matches the solar spectrum. Xenon is too rich in the blue, deficient in the red, and has strong peaks in the 800-900 nm range, leading possibly to large errors in measuring tandem cells, since it may overexcite the first cell and underexcite the second. ELH lamps, with their strong peak in the 500-700 nm range, can give totally misleading results, overestimating some and under-estimating other cells. We have observed both over- and under-estimates using ELH lamps, depending on the kind of tandem cell. Given the non-availability of any reliable simulator, we have decided to rely on global spectrum outdoor measurements under conditions of low humidity, low turbidity, high intensity (90-110 mW/cm^2 at sea level) and moderate temperatures (20-30°C). While not perfect, these conditions are at least reproducible within a few percent all over the country at low elevations. Also, since we make solar cells and not simulator cells, it makes sense to make real-life outdoor tests. Our measurement procedure is addressed in greater detail in Appendix B.

TABLE 5-2. DEPOSITION PARAMETERS FOR SAMPLE 1676 a-Si/a-Si Ge TANDEM CELL

1st Cell (a-Si):

1. p+ layer:

   Eg = 1.9 - 2.0 eV
   t = 100 A - 200 Å (estimate)
   $B_2H_6/(SiH_4 + CH_4) = 0.7\%$
   Power = 30 mW/cm^2
   T = 200° C
   p = 200 μm Hg
   Power = 30 mW/cm^2

2. I_1 layer:

   Grade Bandgap over 4.0 minutes
   Vary SiH_4/CH_4 ratio from 1.25/1 to 1/0

3. I_2 layer:

   T = 220° C
   p = 200 μm Hg
   SiH_4/H_2 = 1/5
   t = 1000-1300 Å (estimate)
   Power = 40 mW/cm^2
   $V_{substrate}$ = -1V

4. n+ layer:

   T = 300° C
   p = 200 μm Hg
   $PH_3/SiH_4 = 2\%$
   time = 4m
   Power = 35 mW/cm^2

2nd Cell:

5. p+ layer:

   T = 300° C
   p = 200 μm Hg
   SiH_4/CH_4 = 1/1 (Eg ~ 1.8 eV)
   $B_2H_6/(SiH_4 + CH_4) = 1\%$
   t = 150-200 A (estimate)
   Power = 25 mW/cm^2

6. I_1 layer:

   T = 300° C
   p = 100 μm Hg
   Power = 25 mW/cm^2
   Grade SiH_4/Ch_4 from 2.5/1 to 1/0 over 2.0 mins.

TABLE 5-2. DEPOSITION PARAMETERS FOR SAMPLE 1676 a-Si/a-Si TANDEM CELL (continued)

7. I_2 layer:
   T = 300° C
   p = 200 μm Hg
   Power = 40 mW/cm^2
   GeH_4/SiH_4 = 15%
   $V_{substrate}$ = -10V

8. n+ layer:
   T = 310° C
   p = 200 μm Hg
   Ph_3/SiH_4GeH_4 = 2%
   Power = 35 mW/cm^2
   t = 500-1000 Å (estimate)

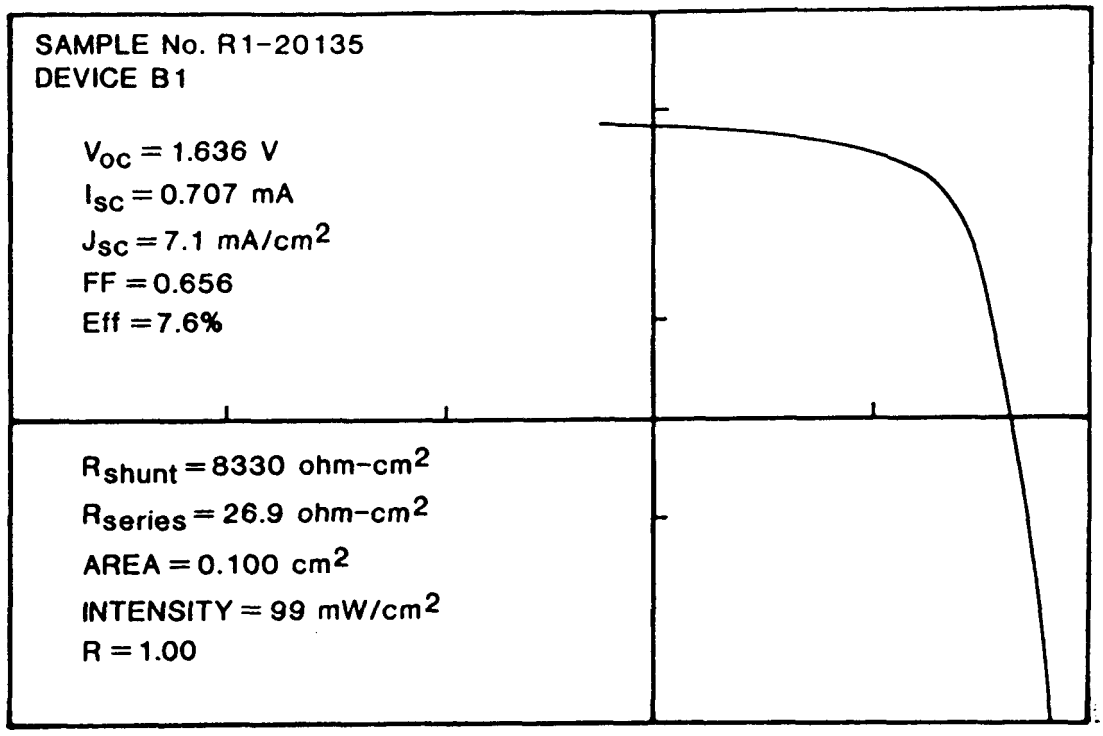

FIGURE 5-1. I(V) CURVE OF a-Si/a-Si TANDEM CELL.

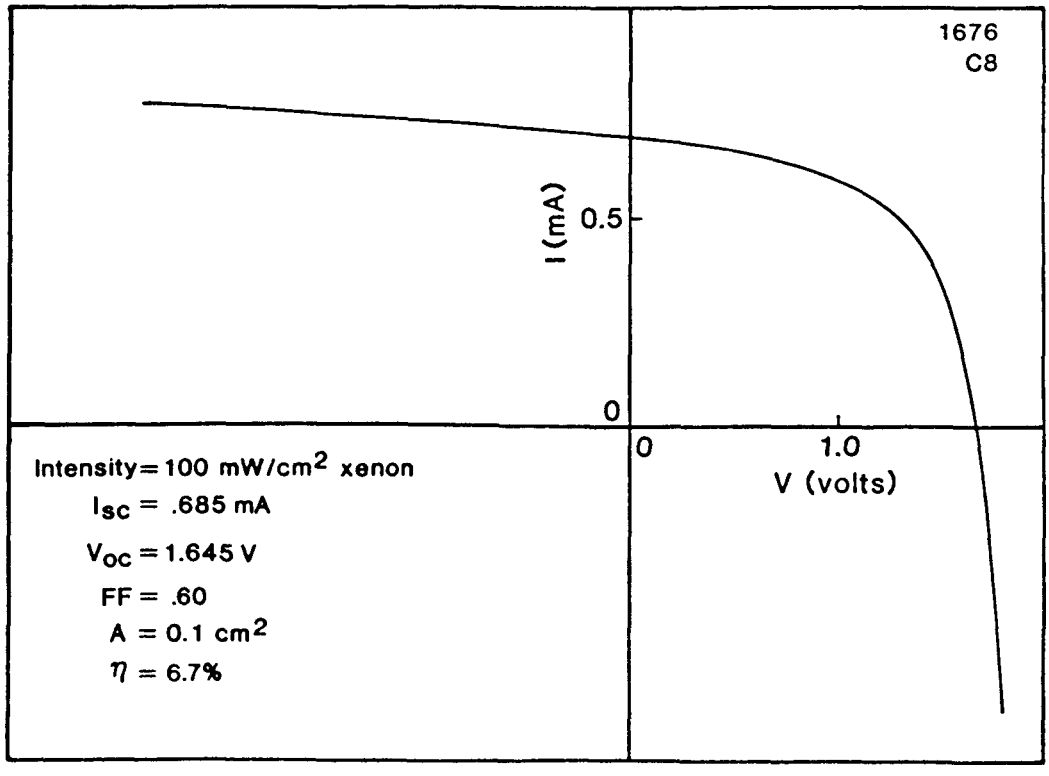

FIGURE 5-2. I(V) CURVE OF a-Si/a-(Si,Ge) TANDEM CELL.

REFERENCES

1. "Research on High Efficiency Stacked Multi-Junction a-Si Alloy Thin film Solar Cells," Annual Report, Spire Corporation (November 1984).

2. "Research on High Efficiency Stacked Multi-Junction a-Si Alloy Thin film Solar Cells," SemiAnnual Report, Spire Corporation (July 1984).

3. P. Vanier, A.E. Delahoy and R. W. Griffith, Proc. AIP Conf. #73 (AIP, NY, 1981) p. 227.

4. D. Carlson, J. Non-cryst. Solids, 35-36, 707 (1980).

5. G. Cody, T. Tiedje, B. Abeles, T.D. Moustakas, B. Brooks and Y. Goldsgtein, J. de Physique, 42, C-4--301 (1981).

6. G. Turban et al., Thin solid Films 67, 309 (1980) and 77, 287 (1981).

7. V. L. Dalal, C. M. Fertmann and E. Eser, Proc. AIP Conf. #73 (AIP, NY, 1981) p. 21.

8. V. L. Dalal, Proc. 17th IEEE Photovolt. Conf. (Orlando, Fl. 1984) p. 86.

9. T. Tiedje, Appl. Phys. Lett. 40, 627 (1982).

10. G. Lucovsky, paper presented at Materials Research Society Meeting, April 1985.

11. K. D. MacKenzie, & W. Paul, Phys. Rev. B (15 Feb. 1985).

12. G. Nakamura et al., J. Non-Cryst. Solids 59-60, 1111 (1983).

13. H. Okamoto et al., J. Non-Cryst. Solids 35-36, 201 (1980).

14. C.C. Tsai, R. Nemanich and M.J. Thompson, Proc. AIP Conf. #73 (1981) p. 312.

15. E. Eser et al., Annual Reort of Chronar Corp. to SERI, (1984).

16. Y. Kuwano and M. Ohnishi, J. de Physique 42, C-4 (1981) p. 1155.

17. S. Wiedeman and E. A. Fagen, Proc. 17th IEEE Photovolt. Conf. (Orlando, FL, 1984) p. 223.

18. T. Tiedje, B. Abeles et al., paper presented at SERI Review Meeting on a-Si (Washington, D.C. 1985).

APPENDIX A

Electronic and Optical Properties of a-(Si,Ge):H Alloys

by

Vikram Dalal, James F. Booker and Mark Leonard

Presented at:
MRS Symposium
Materials Issues in Applications of
Amorphous Si Technology
April 1985

ELECTRONIC AND OPTICAL PROPERTIES OF a-(Si, Ge):H ALLOYS

VIKRAM DALAL, JAMES F. BOOKER AND MARK LEONARD

Spire Corporation
Patriots Park
Burlington, MA 01730

ABSTRACT

We describe the preparation and electronic and optical properties of amorphous (Si, Ge) alloys. A-(Si, Ge):H alloys were prepared by glow discharge decomposition of SiH_4 and GeH_4. The bandgap was varied between 1.78 and 1.42 eV by changing the GeH_4:SiH_4 ratio in the gas phase. We find a distinct influence of growth temperature on electronic properties. Films grown at low temperatures (200-250C) tend to have much lower photo conductivity than films grown at higher temperatures (300-325C). The electron ($\mu\tau$) products of high temperature films are generally $> 1X10^{-7}$ cm^2/V. We also obtain very sharp valence band tails in a-(Si, Ge):H alloys, with slopes of ~ 40 meV. The hole ($\mu\tau$) product is generally $\sim 1\text{-}2X10^{-8}$ cm^2/V. All these properties suffer a catastrophic decline when bandgap is reduced below about 1.5 eV.

Introduction

Alloys of a-Si:H and a-Ge:H have potentially useful electronic properties, particularly in solar energy conversion. The bandgap of such alloys can be varied over a range of 1.1 - 1.75 eV[1], and as such, these alloys are very promising as low gap solar cells in a tandem-junction cell structure.[2-4] However, not much is known about the basic electronic properties of these alloys, such as tail-state densities, mid-gap defects, or electron and hole ($\mu\tau$) products, where μ is the mobility and τ is the lifetime. In this paper, we report some results on these basic electronic properties of a-(Si, Ge):H alloys, and show that the material remains very promising for use in tandem-junction solar cell structures.

Material Preparation

a-(Si, Ge):H alloys were grown by plasma decomposition of SiH_4 and GeH_4 on 7059 glass substrates. GeH_4 used was diluted to 10% in H_2. Typical growth conditions are listed in Table I.

Table I
Growth Conditions

pressure	=: 200-300 μm
T	=: 200-325°C
Flow rate	: 100 SCCM
$(SiH_4 + GeH_4)/H_2$	: 1/6 to 1/7
RF Power	: 50-70 mW/cm^2
Bias on Substrate	: 0 to -100 V
Electrode Geometry	: Triode. Substrate isolated from plasma.

For certain measurements, p-i-n devices were made on SnO_2 coated glass. The configuration was: SnO_2/p/i/n/Al, with light incident from p side. SnO_2 was typically textured with a transmission loss of $\sim$ 20% in 400-500 nm range. The pin devices had a p-type a-(Si, C):H layer, followed by i a-(Si, Ge):H and n+ a-(Si, Ge):H. n+ layer was grown by doping with PH_3 at 1% concentration in the gas phase.

We observed a significant influence of substrate temperature on growth kinetics. Typically, higher substrate temperatures lead to films with high stress, and films which show evidence of etching during growth.[5] Increasing power and substrate negative bias tend to reduce the growth rate, a strong indication of etching, probably by H ions. Further work on etched films is in progress.

Optical Properties

The bandgap of the films was varied from 1.78 eV to 1.42 eV by varying GeH_4/SiH_4 ratio. We decided to stay in this regime because the previous work indicated a catastrophic reduction in electronic properties for Eg < 1.45 eV.[6-8]

In Figure 1, we show a typical $\sqrt{\alpha}$ E vs. E (tauc curve) for an a-(Si, Ge):H film with Eg = 1.57 eV. The bandgap quoted is the intercept of the Tauc curve.

We measured dark (σD) and photoconductivity (σpc) of these films. All films were first annealed at 150° for > 1 hr. to eliminate any variations due to Stabler-Wronski effect. A photoconductivity was measured both under an ELH lamp at 100 mW/cm^2, and under illumination from a He-Ne laser at 1.96 eV. We also measured σpc as a function of light intensity from 5 mW/cm^2 to 100 mW/cm^2 of ELH lamp illumination.

In Figure 2, we show σD and σpc of films grown at 250°C as a function of bandgap. We note that σD is very low, in the range of 10^{-11} S-cm^{-1}, and does not seem to vary significantly with Eg. σ_{pc}, on the other hand, shows a continuous decrease with decreasing Eg.

Quite a different behavior is observed for films grown in 300-325°C range. Figure 3 shows σ_{pc} and σ_D as functions of bandgap. In contrast to Figure 2, we see a systematic increase in σ_D with decreasing Eg., and a relatively flat σ_{pc} curve, until about 1.52 eV, at which time σ_{pc} drops precipitously. Note that even at 1.5 eV, $\sigma_{pc} > 10^{-5}$ S-cm^{-1}, a value high enough for efficient photovoltaic devices.

An important point to note from Figure 2 and 3 is the very high ratio of σ_{pc}/σ_D. This ratio is an indication of material quality, and a high ratio indicates a high electron ($\mu\tau$) product and a low Fermi level.[9] In a-Si:H, we obtain ratios > 10^6, and in a-(Si, Ge):H, ratio > $5X10^4$ for Eg. > 1.5 eV.

In Figure 4, we show the electron ($\mu\tau$) products for 300°C films calculated from σ_{pc} under He-Ne laser illumination. From Figure 4, we see that electron ($\mu\tau$) decreases from $\sim 1X10^{-6}$ cm^2/V for a-Si:H to $\sim 1X10^{-7}$ cm^2/V for a 1.5 eV a-(Si, Ge):H. However, this latter value is quite adequate for a photovoltaic device, since it translates into a field-free diffusion length of $\sim 0.5\ \mu m$, and a range ($\mu\tau E$) of $\sim 5\ \mu m$, assuming an region field of $5X10^3$ V/cm. Thus, electron transport in photovoltaic devices made from a-(Si- Ge):H for Eg. >1.5 eV should not be a problem. Of course, the precipitous decrease in electron ($\mu\tau$) for Eg.< 1.5 eV will make efficient devices in such materials difficult.

We believe that one of the reasons why higher temperatures lead to better a-(Si, Ge):H films is that Ge may introduce structural disorder in the material.[10] As temperature increases, the disorder decreases. However, at higher temperatures (~325°C), H begins to evolve rapidly from the films, and thus, there may be an optimum temperature of ~300°C for growth of high quality films.

Measurement of Valence Band Tail States

To measure valence band tail states, and hole ($\mu\tau$) products, we made pin devices as described in Section 2 above. The technique for measuring valence band tail states was to measure the tail of quantum efficiency (QE) of the device under reverse bias. When the device is under reverse bias, all electron-hole pairs generated by light are collected. Therefore, quantum efficiency is directly proportional to αt, where α is the absorption coefficient, and t is the thickness of the i layer assuming $Xt < 1$, as is the case for small α.[11]

Thus, by measuring the tail of QE vs. photon energy for low energy, (sub-bandgap) photons, we can obtain the tail absorption coefficient α (Uhrbach tail). Since, generally speaking, sub-bandgap absorption occurs from valence band tail states to conduction band,[12] (see Figure 5), $\alpha \sim \exp(E/Eo)$, where E is the photon energy, and Eo is a characteristic slope of the uhrbach tail.[13] Eo is a measure of disorder,[13] and a small Eo means a sharp valence band trail, and low mid-gap defects.

In Figure 6, we plot log QE vs. E, for an a-(Si, Ge):H device of ~1.55 eV i layer, and also show a similar plot for an a-Si:H device with 1.8 eV i layer. Both devices were made at 250°C from gas mixtures diluted at least 5:1 with H_2. We note that both a-Si:H and a-(Si, Ge):H can have sharp valence band tails, indicating low valence band disorder. The value for a-Si:H (38 meV) is the lowest ever reported.

Hole ($\mu\tau$) Product

Hole ($\mu\tau$) product is an important parameter for devices. A high ($\mu\tau$) indicates a high diffusion length. We use the technique developed by Dalal and Alvarez (11) to measure hole ($\mu\tau$). The technique consists of measuring QE of a device under forward and reverse bias and matching the experimental points to a theoretical curve where ($\mu\tau$) is the only unknown. In Figure 7, we plot the experimental points for QE of a 1.6 eV device vs. voltage and also show the analytical curve. From the fit, $\mu\tau \sim 1.5 \times 10^{-8}$ cm^2/V, or a diffusion length of 0.2 μm. Further work on measuring ($\mu\tau$) products for different a-(Si, Ge):H alloys is in progress.

Conclusions

In conclusion, we have shown that a-(Si, Ge):H with high electron and hole ($\mu\tau$) products can be made, and that these alloys have very sharp valence band tails. A catastrophic decline in electronic quality sets in at Eg. < 1.5 eV, which may be due to increased structural disorder due to increased Ge concentration in the alloy.

Acknowledgments

We thank C. Botts and F. Berry for their technical assistance during the course of this work. This work was partially supported by SERI under subcontract ZB-4-03055-1, and by Polaroid.

References

1. J. Chevallier, H. Wieder, A. Onton and C.R. Guarnieri, Solid State Comm. 24, 867 (1977)

2. Y. Marfaing, 2nd European Photovoltaic Energy Conf. (Berlin, 1979) p. 287

3. V.L. Dalal and E.A. Fagen, Proc. 14th IEEE Photovolt. Conf. (San Diego, CA, 1980) p. 1066

4. V.L. Dalal, Proc. 17th IEEE Photovolt. Conf. (Orlando, FLa., 1984) p. 86

5. V.L. Dalal, C.M. Fortmann and E. Eser, AIP Proc. #73, p. 15 (1981)

6. G. Nakamura, K. Sato, Y. Yukimoto, Proc. 15th IEEE Photovolt. Conf. (San Diego, CA, 1982) p. 1331

7. G. Nakamura et al. J. Non-Cryst. Solids, 59-60, IIII (1983)

8. G. Nakamura et al. Proc. of 3rd European PV Solar Energy Conf. (Cannes, France, 1980) p. 835

9. P.E. Vanier, A.E. Delahoy and R.W. Griffith, Proc. AIP Conf. #73, (Carefree, AZ, 1981) p. 227

10. W. Paul & J. McKenzie, Phys. Rev. B, (Feb. 15, 1985)

11. V. Dalal & F. Alvarez, J. de Physique 42, C-4, 491 (1981)

12. G. Cody, in "Semiconductors and Semimetals", Ed. J. Pankove 21B, 11 (1984) (Academic Press, NY)

13. G. Cody et al. J. de Physique 42, C-4, 301 (1981)

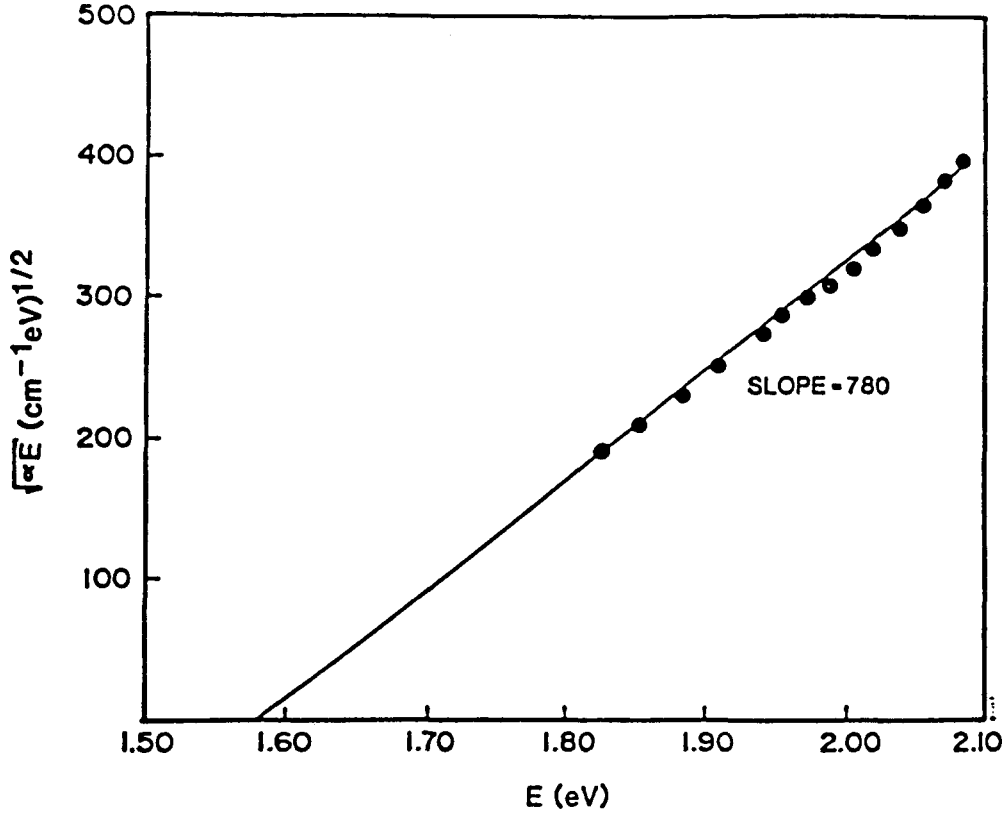

FIGURE 1. ABSORPTION CURVE FOR A-(Si,Ge):H GROWN AT 250°C

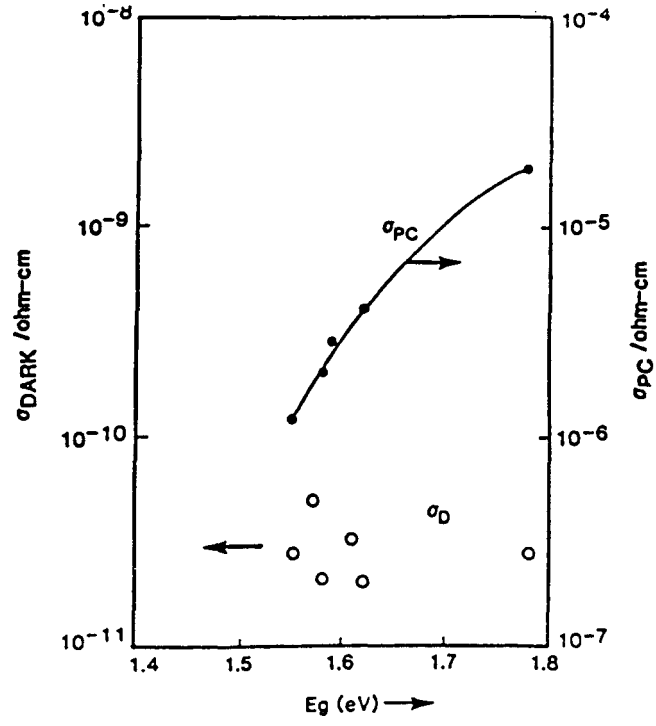

FIGURE 2. DARK AND PHOTOCONDUCTIVITY FOR A-(Si,Ge):H FILMS DEPOSITED AT 250°C

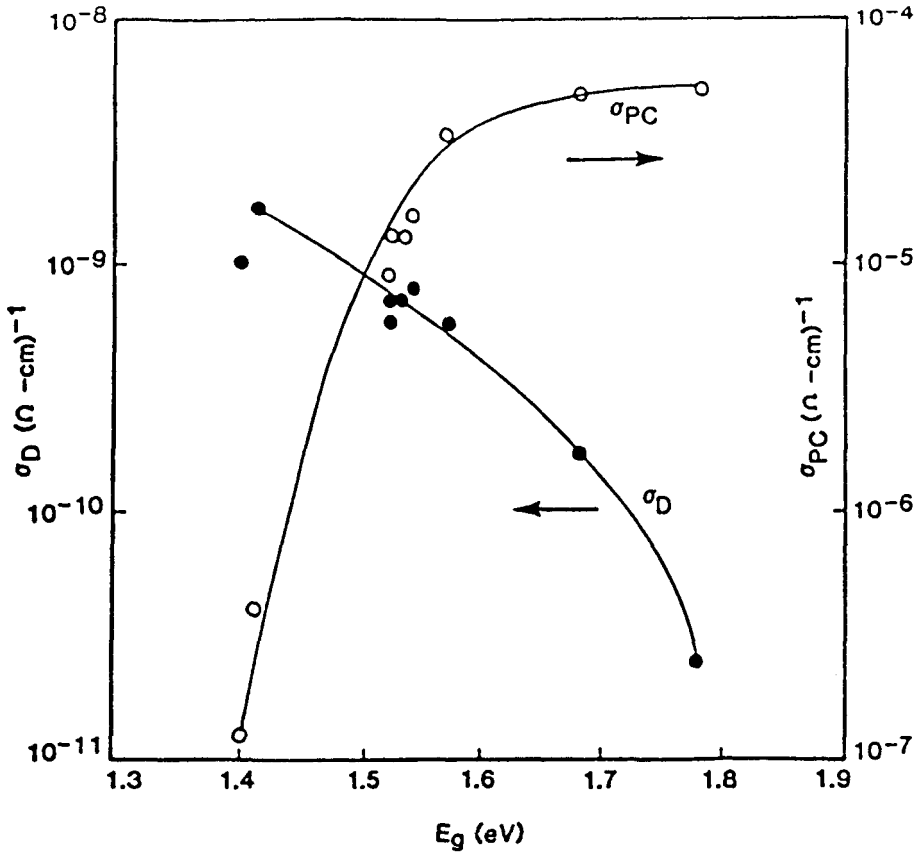

FIGURE 3. DARK AND PHOTOCONDUCTIVITY OF A-(Si,Ge) FILMS DEPOSITED AT 300°C

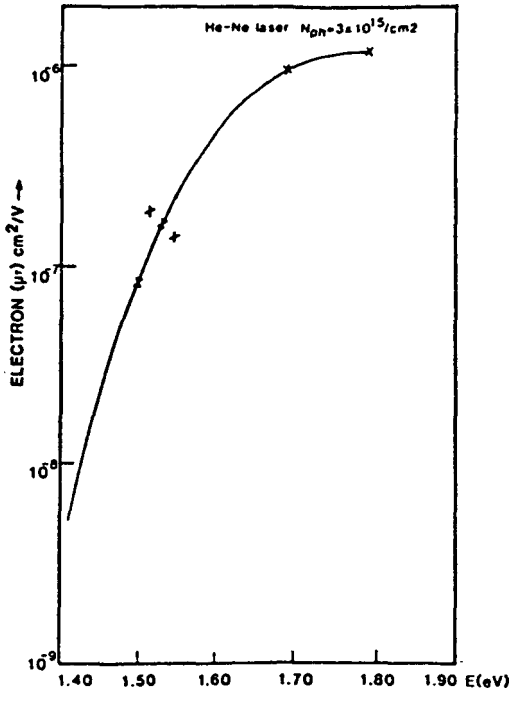

FIGURE 4. ELECTRON ($\mu\tau$) PRODUCT FOR a-(Si,Ge):H FILMS DEPOSITED AT 300°C

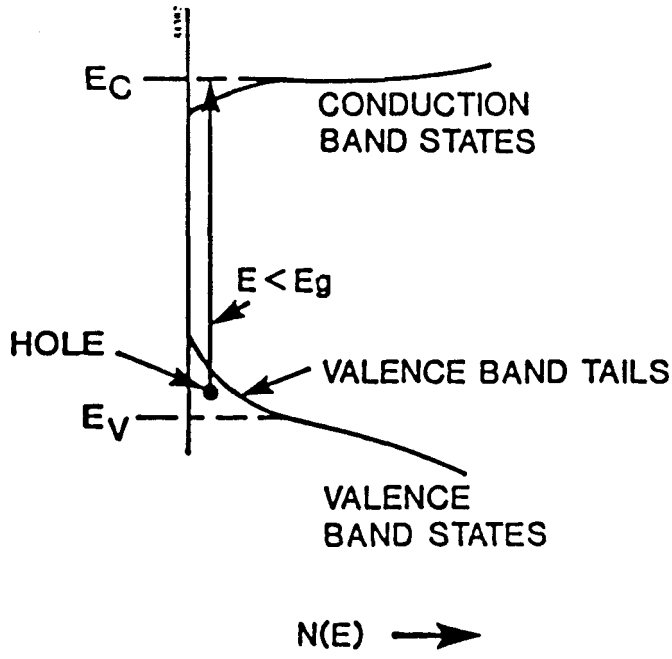

FIGURE 5. A MODEL FOR ABSORPTION FROM VALENCE BAND TAILS

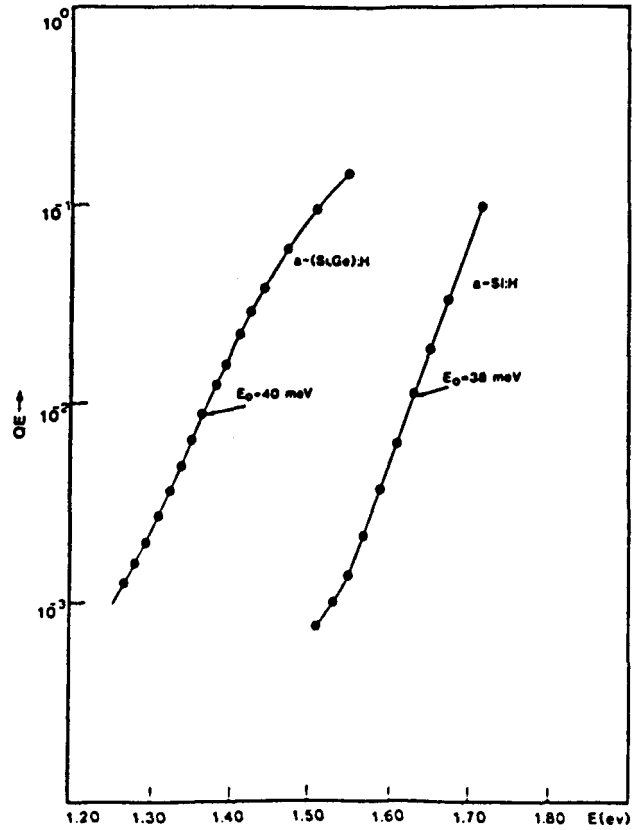

FIGURE 6. PLOT OF LOG OF QE OF PIN DEVICES VS. PHOTON ENERGY

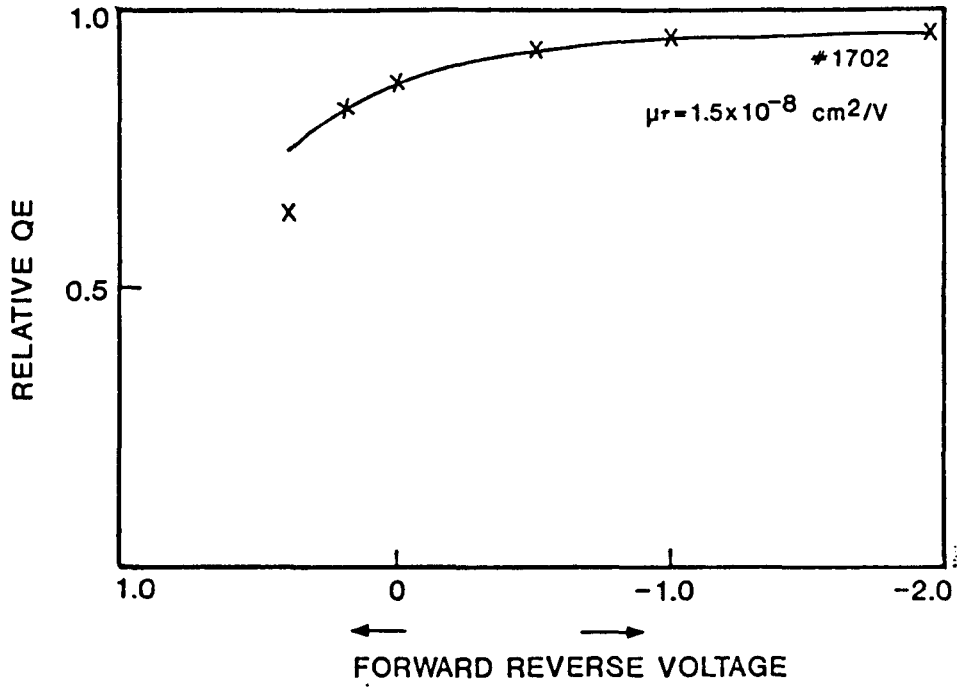

FIGURE 7. PLOT OF QE VS. APPLIED VOLTAGE IN a-(Si,Ge) PIN DEVICE

APPENDIX B
DEVICE MEASUREMENTS PROCEDURE AT SPIRE

The purpose of this Appendix is to describe device measurements at Spire, with special emphasis on calibration procedures.

1.0 DEVICE MEASUREMENTS

The measurements on each sample include current-voltage characteristics, quantum efficiency, and total thickness. The common standard by which cell performance is judged, efficiency under the SERI standard AM 1.5 global spectrum,[1] is determined using I-V and quantum efficiency data. Our detailed procedure, and some of our findings, are discussed following a brief description of our basic measurement techniques.

1.1 OPTICAL PROPERTIES

A Perkin-Elmer model 330 spectrophotometer is used to measure the transmission in the range 700 nm-2500 nm. Sample thickness may then be calculated using the interference peaks in the optical transmission curve. The sharpness of the peaks gives information about the texturing of the SnO_2. Sharp peaks indicate a low degree of texturing.

1.2 CURRENT-VOLTAGE CHARACTERISTICS

I-V curves of our devices are obtained by several methods. The different methods are appropriate for various purposes: quick scanning of cells, hard copies of curves, and calculations using the I-V data are possible. These methods are independent of the simulator we choose to use with a particular cell. A discussion of our simulators is given in Section 2.

1.2.1 Manual Measurement

This measurement allows the user to view the device behavior in any quadrant. A bipolar voltage source serves as the electronic load, with current and voltage each measured by a Keithley 177 Digital multimeter. The analog output of each drives an x-y recorder. The complete apparatus is shown in Figure B-1a.

Our manual measurement is particularly useful in scanning the individual cells on a particular sample. The x-y recorder gives a graph showing details of curvature that would be difficult to display in other forms. The measurement also allows us to quickly scan the individual cells on a sample. The resulting graph (see Figure B-2) becomes part of the permanent record of the sample.

From these curves it is possible to calculate the important device parameters namely, J_{SC}, V_{OC} and FF. Because of the time and inaccuracy involved in calculating these quantities by hand, we typically use a computerized I-V test to determine the parameters. Corrections to the measured short-circuit current (and hence efficiency) are discussed in Section 1.4.

1.2.2 Computer Controlled I-V

This measurement allows us to quickly extract the important device parameters. The setup is similar to that employed in the manual measurement, with the voltage source now

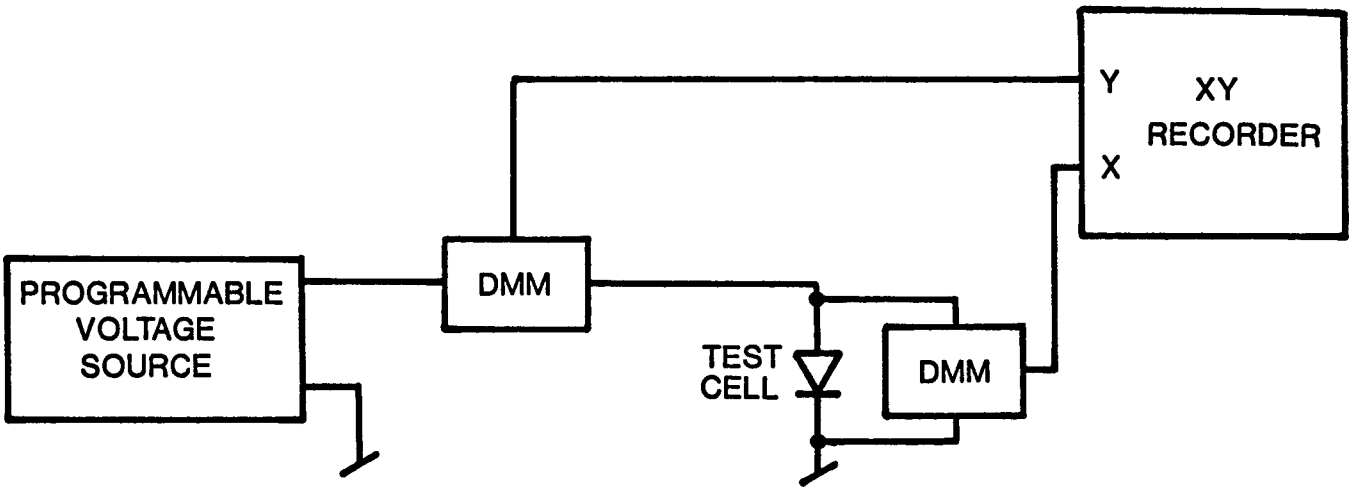

(a)

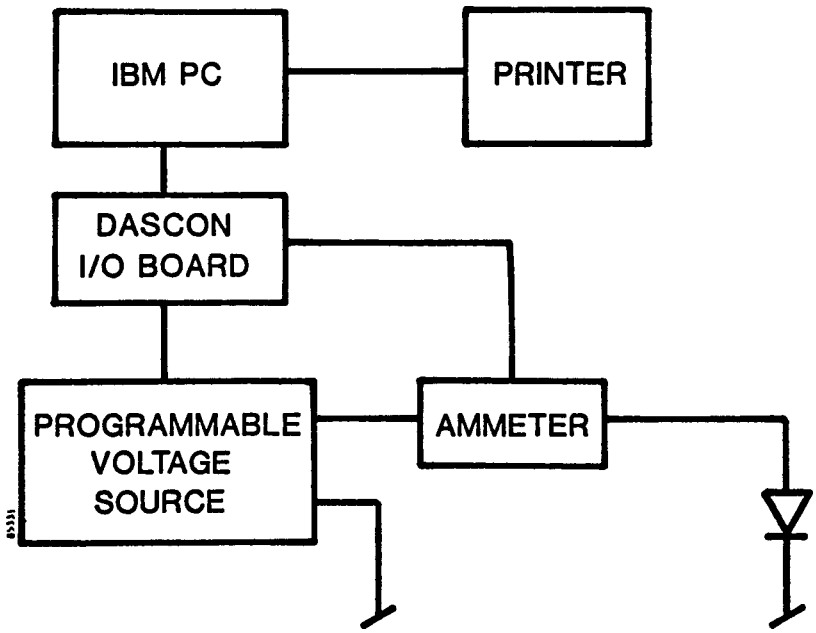

(b)

FIGURE B-1. TEST SETUP FOR (a) MANUAL I-V MEASUREMENTS AND (b) COMPUTER CONTROLLED I-V MEASUREMENTS.

programmed by an analog signal produced by the computer. All computer I/O functions are performed by a MetraByte Dascon-1 board used with a standard IBM Personal Computer. The apparatus is shown in Figure B-1b.

The resulting data can be rapidly manipulated to supply the desired parameters. A typical curve displaying these parameters is shown in Figure B-3. The raw and reduced data is stored on disk for later use.

1.2.3 Curve Tracer

Cells may be connected directly to a Tektronix type 575 curve tracer, allowing instantaneous viewing of I-V characteristics.

1.3 QUANTUM EFFICIENCY

The quantum efficiency of our cells can be measured at wavelengths from 400 to 1000 nm. The measurement can be performed in the dark, or under an ELH light bias of 100 mW/cm^2. The signal light has a bandwidth of 6 nm and is chopped at 85 Hz. It is focused to a spot which falls entirely within our 0.1cm^2 cells, allowing an absolute measurement to be made. The voltage bias on the cell may be varied from -5 to +5 volts.

The entire system is under the control of an Apple IIe microcomputer, allowing for ease of use and high throughput. The interface to monochromator, lock-ins, and voltage bias is provided by an Isaac Data Acquisition and Control System. Figure B-4 shows the apparatus.

Typical data includes the quantum efficiency from 400 nm to 900 nm under 0V-1V bias. From this data, an integrated short-circuit current density (discussed in Section 2.2.3) and the slope of the valence band tail is calculated. Graphs showing quantum efficiency, the ratio of reverse bias to zero bias quantum efficiency, and the log of quantum efficiency (reverse bias) all as a function of wavelength are routinely generated (see Figure B-5). This data is stored on disk for future use.

2.0 MEASUREMENT OF EFFICIENCY

The measurement of efficiency in amorphous silicon alloy cells is difficult because of the varying quantum efficiencies of these cells. Special attention must be paid to the spectral behavior of simulators and reference cells, and appropriate corrections made. Several simulators are described below, followed by a discussion of the errors associated with the use of particular simulators and reference cells. Finally, a comment on measurement of series-connected multiple junction cells is made.

2.1 SIMULATORS

Simulators are used for a variety of purposes, one of which is measuring the efficiency of cells. Because the simulator can have a large impact on the measured performance, it is necessary to make corrections based on the spectral nature of each particular simulator.

2.1.1 ELH Simulators

ELH Lamps can be used as a stable, convenient, and inexpensive light source for a simulator. For these reasons we, and other groups, use such a simulator extensively. Unfortunately, ELH lamps provide a poor match to the solar spectrum. The mismatch is

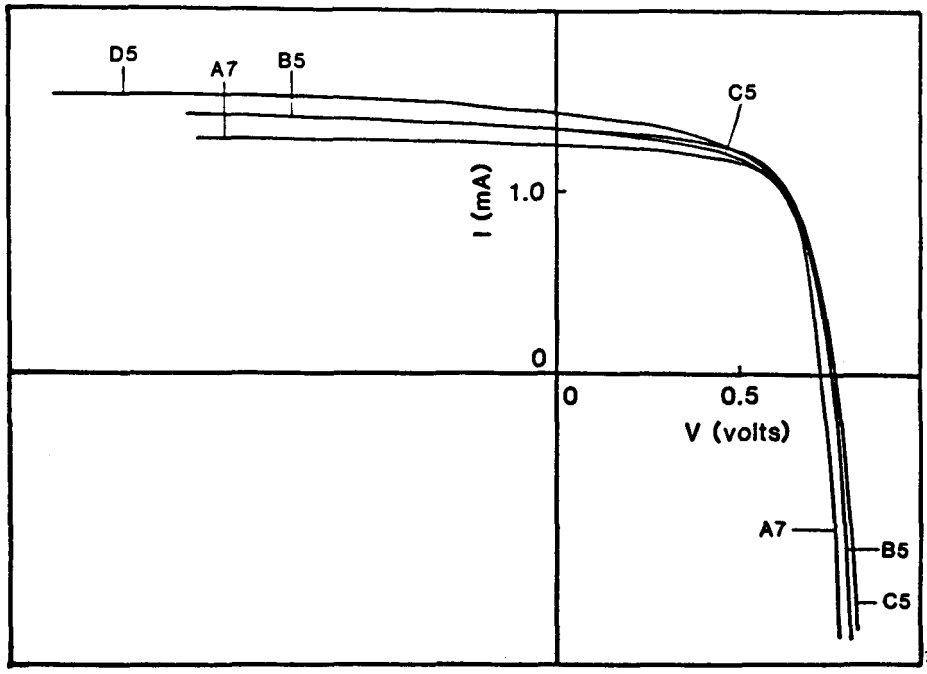

FIGURE B-2. MANUAL I-V MEASUREMENT.

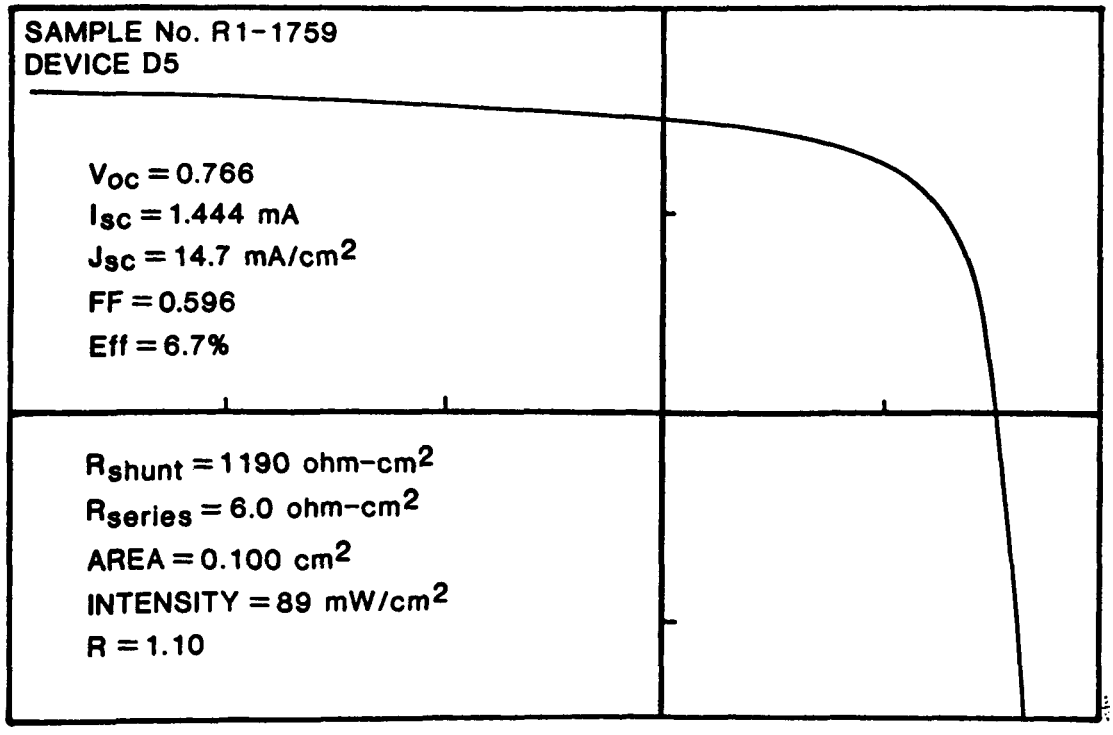

FIGURE B-3. COMPUTER GENERATED I(V) CURVE.

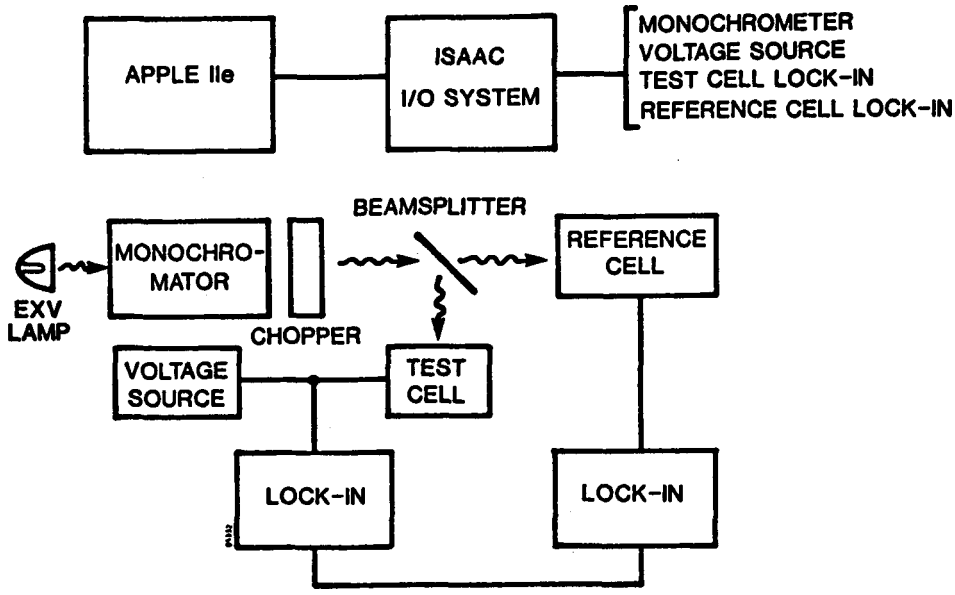

FIGURE B-4. SCHEMATIC SHOWING INSTRUMENTATION FOR QUANTUM EFFICIENCY MEASUREMENT.

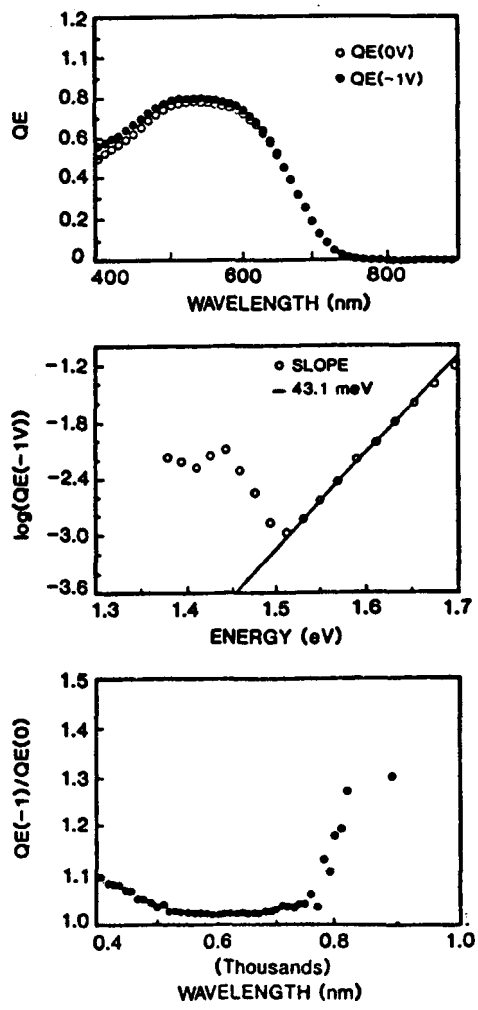

FIGURE B-5. GRAPHS SHOWING QUANTUM EFFICIENCY, RATIO OF REVERSE TO FORWARD BIAS QUANTUM EFFICIENCY, AND LOG OF QUANTUM EFFICIENCY.

severe enough that we find it fruitless to measure tandem cells using this simulator. Moreover, different lamps have significantly different spectra, and individual lamps may change over time. Interpretation of results obtained with such a simulator thus requires great care.

Corrections based on the performance of cells previously measured outdoors, and on calculations of mismatch factors lead to typical downward corrections in short-circuit current of 10% in a-Si:H and 20% in a-(Si,Ge):H cells. The calculations are based on the actual spectrum of the lamp (measured by us with an Optronic spectroradiometer), the SERI AM 1.5 global standard spectrum, the measured quantum efficiency of the particular cell, and the quantum efficiency of our (unfiltered) x-Si reference cell, as discussed below.

Our cells are maintained at a constant temperature by blowing ambient air over the sample. Cell temperatures are thus maintained near 25° C.

2.1.2 ILC Xenon Simulator

Xenon arc lamps with suitable filtering are preferable to the use of ELH lamps. We use on ILC cremax xenon lamp with a KG2 color filter to measure tandem cells. Short-term flickering and lack of uniformity have prevented us from using the lamp on a routine basis. Typical efficiencies of tandem cells found using this lamp source are within 10% of outdoor measurements. Calibration of the lamp is performed using cells previously measured outdoors.

The simulator will be modified to include in addition a separately filtered ELH lamp or other source rich in the red end of the spectrum. This will allow current matching between the individual cells in a tandem device, and will identify the limiting cell. The effect of current matching on the fill factor can also be measured in this way.

The cells are air cooled to maintain a temperature near 25° C.

2.1.5 Other Xenon Simulators

We have made current and voltage measurements on our cells using a Spectrolab X25 and Oriel 1000 watt simulator. The cells were air cooled in all cases. We have found that use of proper filter sets is particularly important in obtaining reliable results with the Oriel simulator. This is discussed below. The important conclusion is that use of a xenon simulator does not guarantee accurate efficiency measurements.

2.1.6 Outdoor Measurements

We are most interested in the performance of our cells under outdoor conditions. When weather conditions allow, outdoor measurements of V_{OC} and J_{SC} are made. The fill factor found using a simulator is used to calculate the efficiency. The global intensity is found by an Eppley pyranometer. Measurements are made only under carefully selected conditions: ambient temperature near 25°C, low humidity and turbidity, absolutely no light or wispy cloud cover, and intensities of 90-110 mW/cm^2. These measurements are discussed in more detail below.

2.2 PROCEDURES FOR CALCULATING EFFICIENCY

To calculate the efficiency of a solar cell three quantities are needed: open circuit voltage (V_{OC}), short-circuit current density (J_{SC}), and the fill factor (ff). Measurements of

V_{OC} and ff are straightforward and reliable. J_{SC} is more difficult to determine. It is found by normalizing a measured short-circuit current (I_{SC}) with respect to the cell area and the incident light intensity. Measuring cell areas is tedious, but does not ordinarily introduce large errors. Proper normalization with respect to intensity requires knowledge of the detailed spectral nature of the simulator and reference cell. Lacking this information, a measurement of efficiency cannot be considered reliable.

2.2.1 Measurement of V_{OC}

The open-circuit voltage is not strongly dependent on intensity (see Table B-1). The effects which cause difficulty in determining J_{SC} (which varies linearly with intensity) are of only marginal importance in measuring V_{OC}. More important is the temperature dependence of the voltage. Because V_{OC} decreases with increasing temperature (T) and I_{SC} increases, it is clearly important that the two quantities be measured at the same temperature. The efficiency of a-Si devices may either increase or decrease with T, so it is important to report the actual measurement temperature.

2.2.2 Fill Factor

As shown in Table B-1 the fill factor shows only a 1% change when the intensity is varied by 10% from 100 mW/cm^2. We thus feel justified in using the ff obtained in indoor measurements with V_{OC} and J_{SC} from outdoor measurements to determine the efficiency.

TABLE B-1. DEPENDENCE OF V_{OC}, FILL FACTOR, AND SERIES RESISTANCE ON INTENSITY. R_{series} is composed of intensity dependent and independent terms. The constant term is the total contact resistance.

Intensity (mW/cm^2)	V_{OC} (volts)	ff	R_{series} ($ohm\text{-}cm^2$)
68	.764	.656	9.1
91	.768	.654	7.5
101	.769	.646	6.5
111	.770	.640	6.1

2.2.3 Short-circuit Current Density and the Use of Mismatch Factors

Defining a simulator's light intensity and its equivalent standard spectrum intensity is the real problem in measuring J_{SC}, and hence the efficiency of cells. The standard practice of using a solar cell as a reference to measure the intensity works well in cases where the quantum efficiency of the cell under study matches that of the reference cell. Unfortunately, when working with amorphous silicon alloys, this is almost never the case. Worse, because the quantum efficiencies of the test cells vary widely, the mismatch between reference and test cell varies from cell to cell. It is clear that a systematic method, incorporating the detailed spectral behavior of both cells, must be used in making the proper corrections.

It is obviously necessary to rely on simulators with non-standard spectra for the majority of our measurements. Our approach is to use the test cell quantum efficiency and information about the spectral characteristics of reference cell and simulators to allow calculation of the efficiency expected under the standard AM 1.5 global spectrum.

When the absolute quantum efficiency of the test cell is known, a simple integration with the standard spectrum gives J_{SC}. When only a relative quantum efficiency is known, then a "spectral mismatch factor"[2] can be calculated to give the error in the uncorrected J_{SC}. This method has been shown to be consistent with the results of outdoor measurements. We have performed our own tests and have also found the method to be in agreement with our outdoor measurements. Note that the calculation allows one to work backwards to determine the absolute quantum efficiency. Both methods assume that I_{SC} is linear with intensity near AM1 at all wavelengths, a good assumption when QE is measured under bias light of an intensity near AM1.

2.2.4 Results

Using outdoor measurements and mismatch factors it is possible to evaluate various methods of measuring efficiency. We have studied the errors and mismatches obtained when using various light sources and reference cells. The results are summarized below.

First, we show in Table B-2 typical errors associated with the use of ELH lamps to measure J_{SC}. An unfiltered x-Si reference cell was used. The results should be regarded as representative of the magnitude of possible errors. One cell (1721) has an extremely peaked quantum efficiency, leading to the very large error. Calculation of mismatch factors gives similar results. Quantum efficiencies of the cells shown below are given in Figure B-6.

TABLE B-2. SHORT-CIRCUIT CURRENT DENSITY OUTDOORS AND UNDER ELH ILLUMINATION. Cells 1609 and 1721 are a-Si:H; 1664 and 1682 a-(Si,Ge):H.

Sample	J_{SC} (mA/cm^2) Outdoors	ELH	Ratio (J_{SC} (ELH)/J_{SC} (out))
1721C5 (a-Si)	6.4	9.9	1.55
1609B6 (a-Si)	11.8	13.2	1.12
1664B6 (a-Si,Ge)	14.0	16.9	1.21
1682C5 (a-Si,Ge)	13.1	15.6	1.19

As mentioned earlier, the use of xenon simulators does not guarantee a good spectral match. This was proven conclusively by measurements made with an Oriel 1000 watt simulator. The errors associated with the different filter sets are shown below in Table B-3.

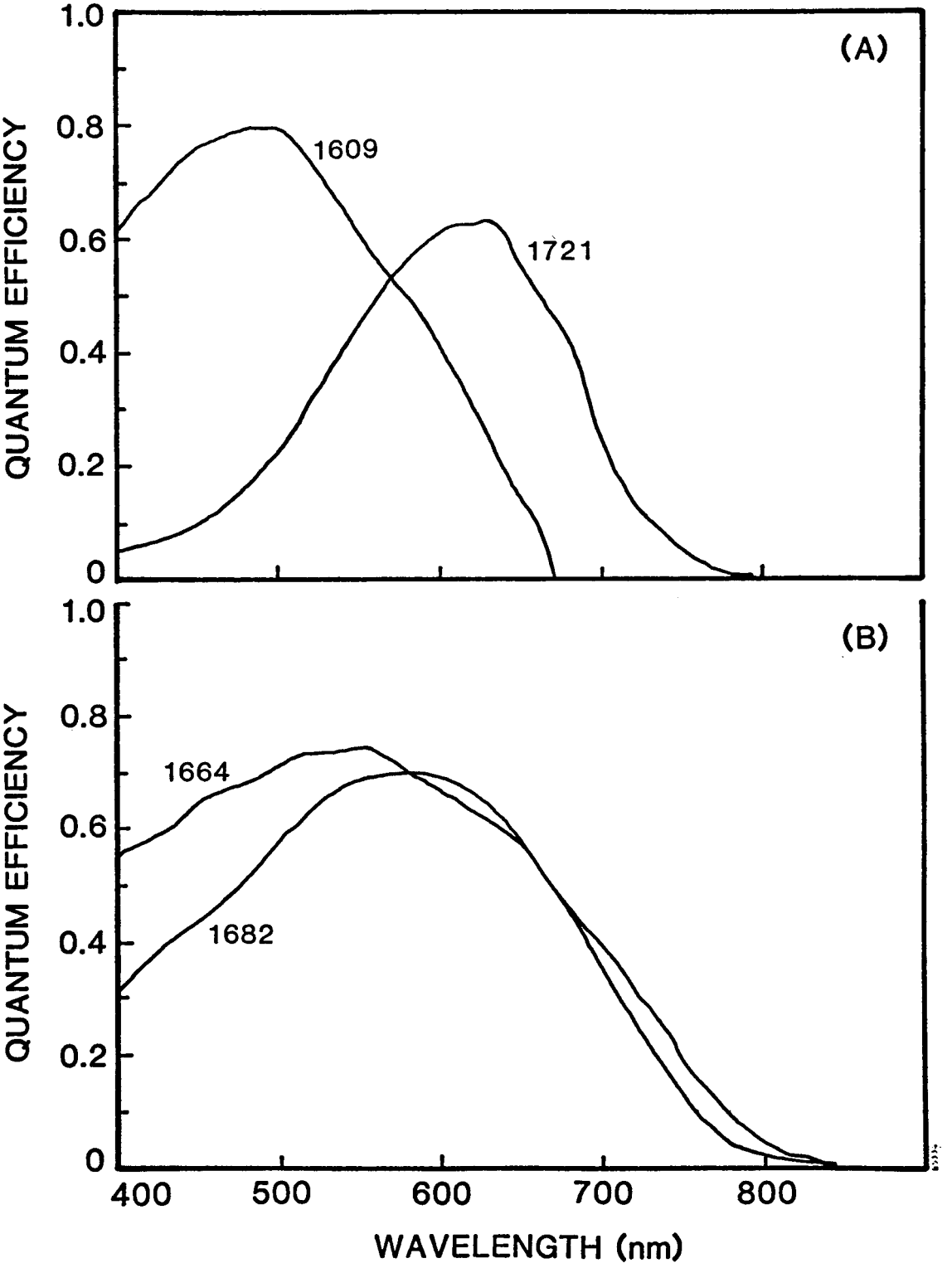

FIGURE B-6. RELATIVE QUANTUM EFFICIENCY OF (a) a-Si:H and (b) a-(Si,Ge):H CELLS

TABLE B-3. ERRORS IN MEASUREMENT OF a-Si CELL WITH ORIEL SIMULATOR.

Filter Set	Ratio (J_{SC} (Oriel)/J_{SC}(out))
AM 1.5 Global	1.24
AM 0 Direct	0.93
AM 1 Direct	0.98
AM 1.5 Direct	0.93
AM 2 Direct	1.08

Mismatch factors calculated using differently filtered reference cells are presented in Table B-4. Quantum efficiencies of the reference cells are given in Figure B-7. The results indicate the typical variability between ELH lamps, and show the difference in mismatch that can be expected with cells of different bandgaps.

TABLE B-4. CALCULATED MISMATCH FACTORS. X25 refers to a Spectrolab X25 simulator, ELH to a particular ELH lamp.

Test Cell	Reference Cell	Mismatch with Simulator X25	ELH
1609	unfiltered	1.09	1.09
(a-Si)	filtered	1.02	.96
1664	unfiltered	1.03	1.17
(a-Si,Ge)	filtered	1.03	1.03

2.2.5 Discussion

The results confirm the large errors possible in the use of ELH lamps, show the effect of varying filter schemes used with xenon and ELH lamps, and show the difficulties in using any single reference cell to approximate the quantum efficiency of a "typical" a-Si cell.

The possibilities for significant error in the measurement of J_{SC} make it imperative to report a mismatch factor whenever a simulator is used. The alternative is to report only those measurements made outdoors under the conditions given above. In this case, the actual conditions should be given in as much detail as possible so that the actual spectrum can be estimated.

2.2.6 Note on Multiple Junction Cells

Series connected multiple junction cells introduce unsolved problem to the measurement of their efficiency. The requirement of current matching between cells introduces an additional constant that prevents use of mismatch factors. Moreover, the errors introduced by non-ideal spectra may be greatly magnified by this requirement. The use of xenon simulators may be problematic because of the response of the tandem cells to wavelengths to 800 nm. Until this problem is adequately addressed, reliable efficiency

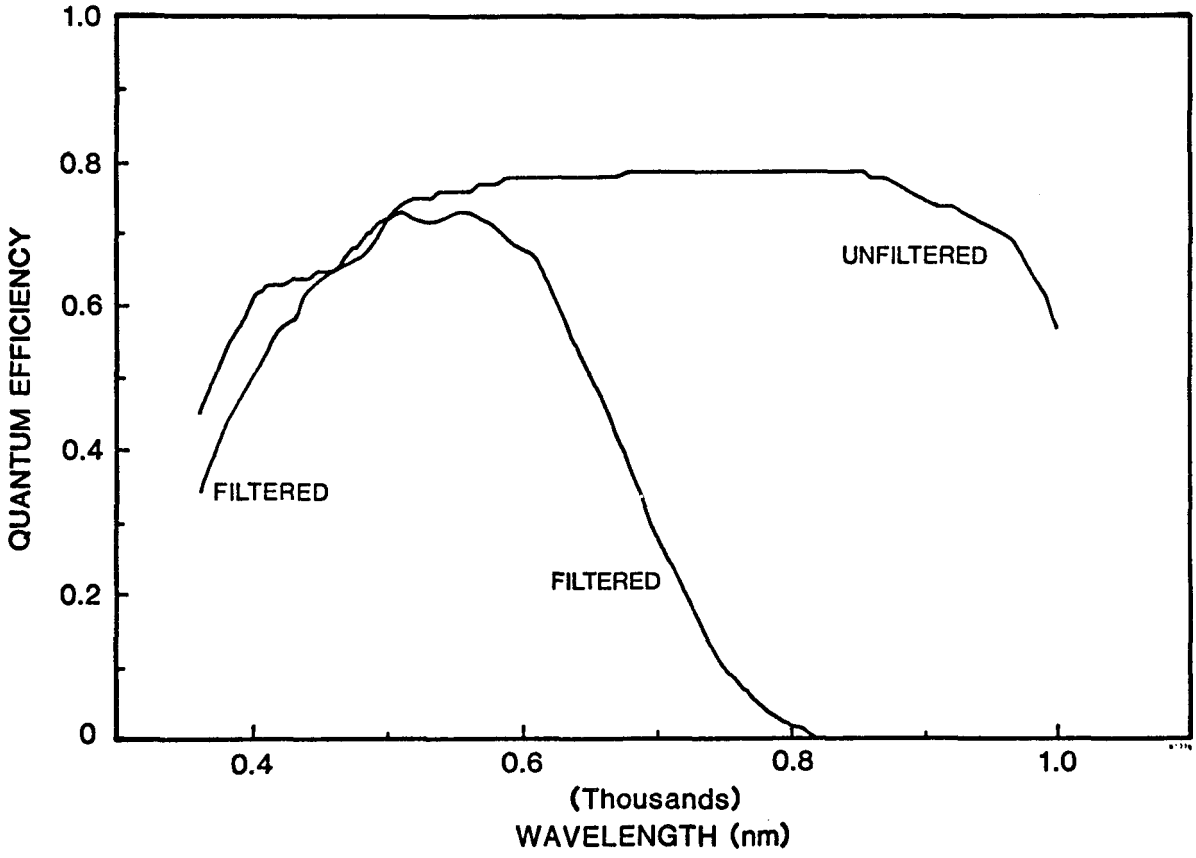

FIGURE B-7. QUANTUM EFFICIENCY OF FILTERED AND UNFILTERED x-Si REFERENCE CELLS.

measurements can only be performed outdoors under conditions of low humidity and turbidity, moderate temperature (20 °C) and high intensity (90 mW/cm^2 at sea level). As discussed earlier, this is a reliable and reproducible measurement at sea level. Conditions for other elevations may have to be appropriately defined. All our tandem measurements are currently verified with such an outdoor measurement.

REFERENCES:

1. R. E. Bird and R. L. Hulstrom, Terrestrial solar data sets. Solar Energy 30, 563-573 (1983).

2. C. H. Seaman, Calibration of solar cells by the reference cell method - the spectral mismatch problem. Solar Energy 29, 291-298 (1982).